Spring 2023

Development and Praxis of Ph Drug Delivery System Contra Zika

Julissa Rodriguez

DEVELOPMENT AND PRAXIS OF PH DRUG DELIVERY SYSTEM CONTRA ZIKA

by

JULISSA RODRIGUEZ

(Under the Direction of James Carter, Ph.D.)

ABSTRACT

As the effects of global warming continue to spread throughout the world, another critical issue is slowly gaining attention in many urban tropical countries. The Emerging Infectious Diseases/ Pathogens list from the National Institutes of Health (NIH) listed the Zika virus as a potential pandemic threat. In 2015, an outbreak of Zika was noted in several South American countries until the spread reached an all-time high of 87 countries in 2017. During the outbreaks, adults affected were noted to have joint and muscle pains, fevers, and rashes. The worst cases reported would ultimately lead to Guillain-Barre symptoms. Still, pregnant women were most affected as their children were born with microcephaly causing the baby's brain to not grow properly. Yet many in the US do not fully comprehend the importance of this situation. The threat of Zika virus reaching the US is not as low as many would choose to believe. The main vector-carrier of Zika virus, Aedes aegypti, is well-known to travel long distances and survive in humid, tropical climates. Many can be found in southern states within the US such as Texas, Florida, and Georgia. The threat increases as there currently is no available vaccine or medication available to combat the Zika virus. Due to this, our research proposes the use of novel biodegradable polymeric micelles as a method of drug delivery for antiviral drugs. The antiviral drugs which will be tested are Dragmacidin derivatives. The proposed polymer methyl (polyethylene glycol)-Poly (β-amino ester) (MPEG-PAE) was synthesized through a Michael-type step polymerization resulting in an amphiphilic block copolymer. These nano-sized polymeric delivery systems are composed of a hydrophilic MPEG and a pH-responsive PAE center. The use of amphiphilic block copolymers has attracted attention as a promising biomedical application for drug delivery due to its ability to self-assemble in specific circumstances. Specifically, the MPEG-PAE copolymer undergoes thermal-induced self-assembly at 50ºC for the formation of micelles. The antiviral compounds listed above will be encapsulated in the newly synthesized pH-responsive micellar nanoparticles and used to suppress Zika virus in cell culture through the inhibition of viral replication.

INDEX WORDS: Drug delivery system, Zika virus, Dragmacidin derivatives, amphiphilic block polymers, methyl (polyethylene glycol)-Poly (β-amino ester), pH-responsive micellar nanoparticles

DEVELOPMENT AND PRAXIS OF PH DRUG DELIVERY SYSTEM CONTRA ZIKA

by

JULISSA RODRIGUEZ

B.S., Georgia Southern University, 2021

A Thesis Submitted to the Graduate Faculty of Georgia Southern University in Partial Fulfillment of the Requirements for the Degree

MASTER OF SCIENCE

COLLEGE OF SCIENCE AND MATHEMATICS

DEVELOPMENT AND PRAXIS OF PH DRUG DELIVERY SYSTEM CONTRA ZIKA

By

JULISSA RODRIGUEZ

Major Professor	James Carter
Committee	Shainaz Landge
	Ji Wu

Electronic Version Approved:
May 2023

DEDICATION

For Mami and Papi, Angelina Giovana Gonzalez and Noe Guadalupe Herrera, for always loving and believing in me and teaching me to always stay curious.

ACKNOWLEDGMENTS

The author would like to acknowledge the following for their time and assistance:

Dr. James Carter for accepting my initial request to be a part of this project and for all of the assistance and knowledge that he shared with me throughout the entirety of this experience that will continue to follow me in my future.

My thesis committee, Dr. Shainaz Landge and Dr. Ji Wu for helping me and teaching me how to continuously improve beyond what I knew I could.

Dr. Michele McGibony and all the Georgia Southern University faculty in the Biochemistry and Chemistry building for all their guidance during my time here.

The Graduate Student Organization for their funding for the research as well as the Department of Chemistry and Biochemistry Georgia Southern University for providing access to the variety of resources and facilities that were required and used for this project.

My Lab Partners: Maria Blahove, Janae Culmer, Maxwell Wallace, Briany Santos, Kesi Domingo, Asa Waterman, and Ethan Rowe for all their teachings and encouragements from beginning which helped me to keep trying.

The other graduate students in no particular order: Nadia Singleton, Emmanuel Fasusi, Igberaese Festus-Ikhuoria, Parker L. Williams, Ayangaifiok M. Akpan, and Austin Seymour for the friendship that we were able to form as we encouraged each other to keep trying and to continue pushing forward during the good, the bad, and the tiring moments.

TABLE OF CONTENTS

Page
ACKNOWLEDGMENTS……..…….3
LIST OF FIGURES…..……...…5
LIST OF FORMULAS...…….……6
LIST OF TABLES…..…..……7
CHAPTER
1 INTRODUCTION……8
1.1 The Concept of Virology……...…….……...8
1.2 Overview of *Flaviviridae* Family……..9
1.3 The Flavivirus Genus……..…9
1.4 *Aedes* Mosquitoes……10
1.5 Zika Virus……...……10
2 NANOPARTICLE DESIGN AND APPROACH……...……...13
2.1 Introduction to Biodegradable Polymers……13
2.2 Diblock mPEG-PAE……13
2.3 mPEG-PAE Micelles……...……14
2.4 Thermal-Induced Self-Assembly of Polymeric Micelles……15
3 INTRODUCTIONS OF ANTIVIRALS……...……...16
3.1 Antiviral Drugs……16
3.2 Dragmacidin Analogs……..16
3.3 Rilpivirine Hydrochloride……17
4 DRUG-LOADING OF POLYMERIC MICELLES……...18
4.1 Introduction to Drug-Loading of Polymeric Micelles……18
4.2 Topological Polar Surface Area……...…18
5 CELL CULTURE BASE SUPPRESSION……20
5.1 Vero Cell Line…….…….20
5.2 Dose Dependence Assay…….…….20
5.3 Plaque Assay……21
6 MATERIALS & METHODS……...…….…….22
7 DATA & RESULTS……...……....26
8 DISCUSSIONS…..……..28
9 CONCLUSION & FUTURE OUTLOOK……..28
REFERENCES……..45

LIST OF FIGURES

Page

Figure 1: Schematic representation of a standard *Flavivirus* virus[17]……..……...32
Figure 2: A 2017 estimate map of the potential range of *Aedes aegypti* in the U.S.[26]……..32
Figure 3: Zika virus replication life cycle[17]…….……..33
Figure 4: General scheme of an AB diblock formation…….33
Figure 5: Poly (ethylene glycol) methyl ether acrylate synthesis[40]…..…...……..33
Figure 6: Poly (*β*-amino ester) synthesis. …..……...34
Figure 7: Michael-type step polymerization of mPEG-poly (*β*-amino ester) [40]…..……..…34
Figure 8: General scheme of the self-assembly process of the AB diblock copolymer[48]…….34
Figure 9: Drug-loading process of the newly formed amphiphilic micelle[48]…….……...34
Figure 10: Synthesis scheme of Bisindole iperazine…….……35
Figure 11: Synthesis scheme of Bisadenine Piperazine…….……35
Figure 12: Synthesis scheme of Rilpivirine Hydrochloride……...……35
Figure 13: Comparison of the two drug-loading determination methods[72,73]…..……..35
Figure 14: A 200 μm microscopic image of a monolayered Vero cell[95]…..……...……..36
Figure 15: FTIR analysis of mPEG-PAE synthesis at different points of the synthesis……36
Figure 16: FTIR of Bisindole Derivative ……..……37
Figure 17: FTIR of Bisadenine Derivative……38
Figure 18: UV-Vis blank mPEG-PAE micelles vs Bisadenine-Loaded mPEG-PAE……..….39
Figure 19: The zeta potential of the bisadenine-loaded mPEG-PAE micelles …….39
Figure 20: Dynamic Light scattering of the Bisadenine-loaded mPEG-PAE micelles…….40
Figure 21: UV-Vis blank mPEG-PAE micelles vs Bisindole-Loaded mPEG-PAE……..40
Figure 22: The zeta potential of the bisindole-loaded mPEG-PAE micelles…….41
Figure 23: Dynamic Light scattering of bisindole-loaded mPEG-PAE micelle……41
Figure 24: UV-Vis blank mPEG-PAE vs Rilpivirine Hydrochloride-Loaded mPEG-PAE..…...42
Figure 25: Dynamic Light scattering Rilpivirine Hydrochloride-loaded mPEG-PAE micelles…42

LIST OF FORMULAS

Page

Formula 1. Drug Loading Capacity of Drug using TPSA…….43

LIST OF TABLES

Page
Table 1: The calculated TPSA for the drugs calculated……45

CHAPTER 1
INTRODUCTION

1.1 The Concept of Virology

From the beginning of human history, there have been three essential components that have contributed to its development[1]. There are three essential components that have contributed to the development of human evolution: 1) human conflicts, 2) environment changes, and 3) infectious diseases[1]. Although historians have identified pandemic diseases since the beginning of written history, the source was not identified until the early and mid-twentieth century[2]. Prior to then, diseases were believed to originate from an individual's sins and deemed as a punishment[2]. The word virus comes from the Latin meaning 'poison' or 'slimy matter'[2]. The establishment of microbiology in 1857 through Louis Pasteur discovery of the specificity of microbial fermentation, would eventually lead to the discovery of viruses[3].

Viruses are microscopic infectious agents of small size, ranging from 20 to 200 nm, and simple composition[4]. They consist of a short sequence of nucleic acid, either DNA or RNA, enclosed within a protein shell known as a capsid and are unique as they cannot replicate on their own. They invade a host cell and proceed to use the components of the infected cell in order to commence viral replication[4, 5]. Viruses often kill the host cell after replication, causing damage to the host before infecting surrounding cells[6]. However, the concept of a virus was difficult for scientists to grasp at that time period due to the inability to see such a small molecule with the naked eye. By the early 19th century, studies on the tobacco mosaic virus would eventually change this mindset and lead to the establishment of virology[3, 7].

Virology is the branch of microbiology that focuses on the study of viruses[8]. The historiography of virology is believed to have emerged from the work contributed by Dimitri Ivanovsky (1892) and Martinus Beijerinck (1898) on the transmission of tobacco mosaic virus[1, 3, 7]. The work of Ivanovsky and Beijerinck demonstrated that the agent producing the mosaic disease in the tobacco plants was able to pass through porcelain ultrafilters that were impermeable to bacteria[3, 8]. By 1935, the tobacco mosaic virus would become the first virus to be crystallized[3]. Eventually, direct visualization would be possible in 1940 through the electron microscope securing the establishment of virology[3]. Interest in virology was further fueled by the important plant and human diseases such as smallpox, influenza, and AIDS. The development of virology continues to grow through interest in preventative measures against viral infections, such as vaccines, which require further research.

Viral hemorrhagic fevers (VHFs) are a group of viral diseases that affect multiple organs of the human body[9]. Hemorrhage is large amount of bleeding from damaged blood vessels. The decrease in circulating blood flow capacity causes a stress on the cardiovascular system by decreasing blood pressure and decreasing perfusion pressure of tissue blood flow[9]. VHFs are caused by viruses from the four families: *Arenaviridae, Bunyaviridae, Filoviridae,* and *Flaviviridae*[10]. The majority of these viruses exist through vectors such as arthropod-borne or rodent-borne infections[10]. Afterwards, they are transmitted from human-to-human interactions

which contributes to their widespread outbreaks[11]. The critical aftereffects of VHFs are the overall damages towards the cardiovascular system and the decrease in the body's ability to function independently[9]. A shared characteristic of VHFs is that they are generated by RNA viruses whose constant mutations are noted to contribute to the emergence of diseases[9]. The majority of VHFs currently have no known vaccine or drug treatment available[9]. The growing rate of climate change, globalization, and international travel raises the population risk of spread for VHF viruses[9].

1.2 Overview of *Flaviviridae* Family

Flaviviridae are one of the four main groups of viral hemorrhagic fevers (VHF) whose name originates from the Latin word flavus or yellow, in commemoration of the yellow fever virus[12, 13]. Various epidemics throughout history are perceived to be associated with members of the *Flaviviridae* family since as early as the 1600s[14]. The *Flaviviridae* family is composed of positive, single-stranded, enveloped RNA viruses[1]. These viruses are found predominantly in arthropods such as ticks and mosquitoes, infecting birds and occasionally humans[1]. There are currently four principal members of the genera *Flavivirus, Pestivirus, Hepacivirus,* and *Pegivirus*[12]. Members of the *Flaviviridae* family are classified based on distinct viral characteristics and replication life cycle. Members of the family have a shared characteristic of 40-60 nm virions containing glycolipids and glycoproteins[12].

Viruses of the *Flaviviridae* family initiate replication through the synthesis of an antigenome which serves as a template for genome RNA production[12]. The genome RNA has three vital functions in the replication cycle: 1) as a messenger RNA (mRNA) for translation of viral proteins 2) a translational template for the synthesis of virion proteins and 3) as a genetic material within immature virus particles equipped for further infection. Afterwards, the viral proteins undergo replication through a complex topography within the endoplasmic reticulum (ER). Once the virions are assembled, they bud into the lumen of the ER where they are secreted through the vesicle transport pathway and released by exocytosis to resume the cycle. Amongst the family members, those associated with the genus *Flaviviruses* are recognized as influential to human and veterinary pathogens[12].

1.3 The *Flavivirus* Genus

Since the initial discovery of the yellow fever virus (YFV), members of the genus *Flavivirus* are acknowledged for their epidemic potential, infecting up to 400 million people annually[15]. There are over 50 members of the genus including pathogens such as yellow fever virus, dengue virus, West Nile virus, Japanese encephalitis and Zika virus[14]. Majority of *Flavivirus* are arboviruses and have two distinct transmission routes: sylvatic transmission cycle and urban transmission cycle[13]. The sylvatic transmission cycle is where the virus circulates between *Aedes* mosquitoes and non-human primates[13]. The urban transmission cycle is where the virus circulates between *Aedes* mosquitoes and humans[13]. The urban transmission *by Aedes*

aegypti is known as the primary cause for the global spread of *Flaviviruses.* The viral particles are nearly circular in shape with a common characteristic of a with a diameter of ~50 nm[13, 15]. The model of a *Flavivirus* virus is composed of an outer protein shell encapsulating the viral RNA (Figure 1)[15]. The positive single-stranded RNA (ssRNA) genome is approximately 10.8 kb with a 5′-terminal type I cap structure[11, 15]. The outer protein shell consists of three main proteins: the capsid (C) protein surrounding the viral genome which is encapsulated by the membrane (M) protein and envelope (E) protein as noted on Figure 1.

The E protein is composed of some fats combined with protein with the proteins sticking out of it. This layer mediates the viral entry steps of the replication cycle for the *Flavivirus* viruses. The membrane (M) protein is originally arranged as a premembrane (prM) protein bonded to the E protein as prM-E spikes facing out. This prevents the E protein from undergoing unwarranted conformational changes that may inhibit viral fusion with host membranes. During the transition of the immature virions through the trans-Golgi apperatus, the prM protein will cleave to an M protein by a serine protease that is required for the mature form of the virion[15]. The C protein is a small helical protein with surfaces that can bind either host lipids or viral nucleic acids which assist in incorporating viral genome into the virion[15].

1.4 *Aedes* Mosquitoes

Infected mosquitoes of the *Aedes (Stegomyia)* genus are acknowledged as the prime vectors for viral propagation of *Flavivirus* viruses[16]. The *Aedes aegypti* is a well-known carrier of a variety of viruses such as dengue virus, yellow fever virus, chikungunya, and Zika virus[17, 18]. Many countries with tropical climates are exceptionally susceptible to diseases as the *Aedes* vectors thrive in these locations[19]. Since the survival of these mosquitoes depends on feeding on mammals, these mosquitoes prefer tropical, urbanized areas[19].

The spread of *A. aegypti*, which is distinguished by long-distance imports, greatly benefits through these factors[4]. A growing concern is the probable influence of climate change with regards to vector-borne mosquitoes[4]. Climate change is expected to influence future disease patterns which will cause a change in the location of vector-borne diseases. Areas that had previously not been exposed to vector-borne mosquitoes may now succumb to the transmission of *Flavivirus* infected mosquitoes[4]. In 2017, the CDC estimated the potential range of spread for *A. aegypti* within the United States which included several southern states including Georgia (Figure 2)[19]. Several infectious diseases including the Zika virus (ZIKV) are mainly transmitted through the infectious saliva of the *A. aegypti* female mosquitos[19].

1.5 Zika Virus

Zika Virus (ZIKV) is an RNA arthropod-borne virus (arbovirus) from the *Flaviviridae* family which is transmitted through *Aedes* mosquitoes[20-22]. First discovered in the Ziika Forest in Uganda in 1947, ZIKV has remained a neglected tropical disease until the recent outbreaks in Latin America from 2015 to 2017[23]. Many people who are infected with ZIKV will either display

no symptoms or will only display mild symptoms such fever, rash, headache, joint point, conjunctivitis, and muscle pain. Additionally, ZIKV was noted to have a connection with several neurological diseases such as microcephaly, and meningoencephalitis, and Guillain-Barre syndrome, a rare autoimmune condition that affects the peripheral nerves. Why should we pay attention to the Zika virus, which has been labeled a "harmless" pathogen since its discovery in1947?

Between 2013 to 2015, the first major outbreak of ZIKV infections was reported in French Polynesia. Cases of newborn infants with neurological disabilities from infected pregnant women were first reported[24]. Eventually, additional reports of adults with neurological complications associated the possibility of ZIKV transmission to the patients[24]. Spread of ZIKV to Brazil is believed to have originated from asymptomatic French Polynesian travelers visiting during the 2014 World Cup. Since then, it is believed that around 500,000–1.5 million people in Brazil have been infected with the ZIKV[24]. The first case of ZIKV infection was reported in April 2015 with approximately 64,311 confirmed cases by the end of 2016[24]. By February 1, 2016, the World Health Organization declared a public health emergency of international concern due to the increasing reports of severe neurologic complications associated with ZIKV infections.

As shown in Figure 3, the viral RNA replication process of ZKV is pH dependent. ZIKV is spread to a human host via the bite of a female *Aedes aegypti* mosquito. Once the host has been infected, the virus will commence viral RNA replication through receptor-mediated endocytosis. Viral fusion commences in the endosome, via a low pH of 5.7, where the nucleocapsid is released into the cytoplasm[15]. The viral genome then travels to the endoplasmic reticulum (ER) where it will bind with the membranes and initiate viral translation. The viral genome will undergo translation, replication, and assembly in ER, at a pH of 7.2, and bud into ER[15]. Immature virions can proceed through the trans-Golgi network where they mature into the infectious virions before initiating budding[15]. Mature virions then undergo exocytosis at a pH of 5.7 and carry on infecting other cells[15].

According to the Centers for Disease Control and Prevention (CDC), there currently is no specific treatment or approved vaccine available for ZIKV[20]. The only method of treatment available recommends treating the symptoms of ZIKV to alleviate any pains or fevers. Due to the absence of any effective vaccines or antiviral treatments, the only current methods available to combat the spread of ZIKV are by reducing contact between arthropod vectors and susceptible humans and elimination or reduction of mosquito populations[25]. However, there are several complications with these methods. Firstly, the insecticides that were effective for the eradication of *A. aegypti* were not environmentally effective due to the highly toxic nature of the insecticides that persist after use[25]. Secondly, the uncontrolled growth of urban development increases the risk of human exposure to *A. aegypti* mosquitoes. Contact between vectors and humans was thus unavoidable due to uncontrolled urban development and the reduction of vector-controlled measures[25]. An increasing concern about ZIKV is its association between infected mothers and microcephaly. Pregnant women infected with ZIKV during the can be passed from the pregnant

women to her fetus as the virus appears to go through the placenta[26]. The ZIKV has been observed to use the paracellular pathway to cross the placenta monolayer by disturbing cellular tight junction. The ZIKV can also use transcytosis, the transcellular transport in which macromolecules are transported to interior of the cell, to cross both the placenta barrier and the blood brain barrier[25].

Infections during pregnancy can cause birth defects causing congenital brain malformations like microcephaly[25, 26]. Microcephaly is a rare condition where a baby's is smaller compared with other babies interfering with the brain growth of a child[26].

ZIKV contributes to microcephaly by inducing neuropathogenesis, the development of diseases of the nervous system. This can occur through a variety of mechanisms, predominately cell cycle dysregulation, immune and inflammatory responses, and neuronal apoptosis[26]. Neuronal apoptosis, mechanism by which a neuron induces its own death, has been observed to be the primary method of cell death by which ZIKV induced developmental brain disorders such as microcephaly[25, 26].

There are no treatments for microcephaly and are usually only detected too late. Although most of the latest outbreak occupied mainly Central and South America, there were 224 reported cases in the US in 2016 most of which were transmitted to Florida and Texas. The escalation of mosquito-borne disease can be attributed to unrestrained urbanization, global warming, and the lack of effective mosquito vector control[20, 23]. Due to the current lack of vaccines and effective mosquito contact preventions, the urgency for an alternative approach is continuously ongoing.

CHAPTER 2

NANOPARTICLE DESIGN

Global outbreaks of infectious diseases have been acknowledged as the primary enemy of human civilization[27]. Recurring epidemics often stem from viral pathogens, such as the yellow fever virus, whose main vectors are mosquitoes. This raises concerns since pathogen-carrying vectors are highly attracted to urbanized areas. Especially in this time period where urbanization and international travel are booming at unprecedented speeds which contributes to the global spread of viruses. However, the current limitations of oral antivirals inhibit the potential for target therapy. A solution that has attracted attention is the use of nanoparticles as drug delivery systems[28]. The biocompatibility and tunable properties of nanoparticles further enhance their prospects as drug carriers while ensuring that there is no decrease in drug potency against the specified pathogen.

2.1 Introduction to Biodegradable Polymers

In the ever-advancing field of nanomaterials, biodegradable polymers have attracted attention as promising instruments for biomedical applications. These polymers are composed of biodegradable and biocompatible monomers that can be modified as stimuli-responsive systems for drug delivery. Biodegradable polymers have advantages over the current therapies available as they can be engineered to be stimulated at a variety of different properties[29]. These stimuli-responsive amphiphilic copolymers containing hydrophilic and hydrophobic segments have garnered attention as suitable drug carriers for hydrophobic and hydrophilic drugs. The biodegradable polymer synthesized will depend on the classification of drug designated. There are a variety of biodegradable monomers available ranging from different shapes, sizes, selectivity, and biocompatibility[28]. Additionally, the biodegradable polymers can break down after use into smaller chemical fragments until they are finally expelled from the body[29]. Due to this, the polymers are safe for use without requiring an additional course of action for withdrawal.

2.2 Diblock mPEG-PAE Polymer

A biocompatible and biodegradable amphiphilic polymer that can satisfy the requirements necessary for a drug carrier specifically designed to transport an antiviral drug towards the Zika virus is mPEG-PAE. The polymeric chain, mPEG-PAE, is named after the two monomer segments merged to form the copolymer: poly (ethylene glycol) methyl ether and poly (β-amino ester). Linear polymer chains that consist of more than one constituent monomer are known as block polymers[29]. Each block is designated a letter beginning with ‘A’ and ‘B’ and so forth depending on the amount of different monomers[29]. The polymer chain, mPEG-PAE, is composed of two distinct monomers and is referred to as an A-B diblock copolymer. The ‘A’ segment refers to the poly (ethylene glycol) methyl ether acrylate or mPEG-A monomer while

the ‘B’ segment refers to the poly (β-amino ester) or PAE monomer. When the A monomer couples with the B monomer, they form the A-B diblock polymer (Figure 4). The polymerization of the A-B diblock requires three main steps. First, the mPEG is acrylated through a synthesis with acryloyl chloride to form poly (ethylene glycol) methyl ether acrylate (mPEG-A) as shown on Figure 5. Triethylamine (TEA) is used to catalyze the reaction with dichloromethane (DCM) as a solvent to dissolve any side reactions. Secondly, hexane-1,6-dioldiacrylate (HDD) was synthesized with 4,4’-trimethylenedipiperidine (TDP) to prodcue poly (*β*-amino ester) (Figure 6).

Lastly, the mPEG-A and the poly (*β*-amino ester) were synthesized using a Michael-type step polymerization to produce the final product of MPEG-poly (b-amino ester) block copolymer as shown in Figure 7[29]. The mPEG block is introduced as the hydrophilic segment which is biocompatible and acts as a protecting group from macrophages and reticuloendothelial systems[29, 30]. The PAE segment attached to the other end acts as the hydrophobic segment and has a pK_b value ~6.5[29]. Due to this, PAE is soluble below a pH of 6.5 at which point it will release drugs when in an acidic environment. When the environment is at a pH above 6.5, PAE is insoluble and will retain its drug-loaded micelle state[29, 30]. This diblock copolymer meets several of the requirements necessary for an antiviral drug-carrier since it is biocompatible and would retain the antiviral drug unless in an acidic environment. For example, the low pH of 5.7 where the Zika virus is known to undergo an acid-catalyzed fusion reaction with an endosome. This is advantageous because the virus is targeted outside of the cell which reduces any chance of viral replication as well as damage to the cell.

2.3 mPEG-PAE Micelles

The growing necessity to improve target therapy intensifies the attraction for drug-loading nanoparticles as they have tunable properties for the required circumstances. The tunable properties of nanoparticles are endless from their selectivity, size, shape, and biocompatibility which enables them to be used for a variety of biomedical applications[31, 32]. From enhancing molecular imaging to detection and diagnostics, nanoparticles are slowly becoming more sought-after alternatives as research journals on their possible applications continue to be published[31]. Polymeric nanoparticles in particular capture the attention of scientists with their abilities to form micelles through self-assembly. These micelles are designed using two distinct segments which form an amphiphilic micelle when stimulated in an aqueous solution (Figure 8). The outer layer of the polymeric micelle mPEG-PAE, is composed of the hydrophilic monomer mPEG which is well known for its non-toxicity, absence of antigenicity and immunogenicity, and ability to prolong its blood circulation time[33]. The inner layer of the micelle is devised of the hydrophobic monomer, PAE, which is known for its pH responsiveness, biocompatibility, and serves as drug reservoirs for hydrophobic drugs[34]. Additionally, these polymeric micelles assist in enhancing the drug concentration due to the enhanced permeability and retention effect[34].

2.4 Thermal-Induced Self-Assembly of Polymeric Micelles

One of the unique features of the amphiphilic block copolymer, mPEG-PAE, is the specific circumstances required to undergo micelle self-assembly. First, the amphiphilic copolymer requires an aqueous solution. This is beneficial to the process for two main reasons: 1) the aqueous solution encourages hydrophobic drugs to plunge within the nano-sized micelles and 2) since the self-assembly process does not require any harsh solvents, the polymeric micelle is biologically friendly and does not require an added purification step. Secondly, the amphiphilic copolymer is thermosensitive and requires a specific temperature to self-assemble. An increase in temperature will instigate the formation of spherical micelles. Once the copolymer is thermally induced, it forms a polymeric micelle that can be utilized as a drug delivery system for hydrophobic drugs (Figure 9). Due to the thermosensitivity of these micelles, the copolymer can undergo self-assembly within the biologically friendly solvent, ultra-pure[35]. Once the two conditions are met, the amphiphilic block polymer will self-assemble to form a nanoparticle micelle that is soluble in pathogenic environments.

CHAPTER 3
INTRODUCTION OF ANTIVIRALS

3.1 Antiviral Drugs

Throughout history, viral diseases have been recognized as the greatest enemy of human civilization. The global mortality rate of viral epidemics on mankind far exceeds the 56.4 million deaths from World War II which is known as the deadliest war in history[27, 36]. In order to fight against the ever-growing list of viruses, scientists have developed antiviral drugs. The boom of a new era of medical treatments arose after the development of Idoxuridine, the first antiviral drug approved for clinical use, in 1963[35, 37]. There are approximately 90 approved antiviral drugs that are categorized into 13 functional groups[38]. Since then, other antiviral drugs have been approved for human use against viruses such as HIV-1, influenza virus, HCV, and most recently to treat COVID-19[27]. Due to the broad classifications of viruses, many of these antiviral drugs are designed to treat specific viral infections. The principal objective of antiviral drugs is to assist the body to fight off viral infections by reducing the harm to the host system and suppression of the virus[27]. Drug design for antivirals is complex and currently concentrates on two main pathways which avoid destroying the target pathogen[37]. Since viruses utilize the host cell for viral replication, designing an effective and safe drug that does not affect the host cell becomes more complicated[37]. Many antiviral drugs operate by targeting the pathway of the pathogen by either targeting the viruses themselves or the host cell factor[37]. Antivirals concentrate on either blocking viral replication or introducing errors to the genetic materials of viruses[27, 37]. Although these approaches have limited leeway, they prove to be the most effective options available for battling viruses. Additionally, biological antivirals are also required to ensure safety, cost, availability, and efficacy before they can be approved for clinical use[27, 37].

3.2 Dragmacidin Analogs

The search for natural products in the marine environment has led to the discovery of a variety of biologically active bis(indole) alkaloids isolated from marine sponge families *Spongosorites, Hexadella,* and *Dragmacidon*[39]. These compounds are reported to have a diverse range of applications which include antifungal, anti-inflammatory, antibacterial, antiviral, and cytotoxic activities[39, 40]. Two dragmacidin analogs were tested to ensure their compatibility with the biodegradable polymeric micelle, mPEG-PAE. The compounds 3,6-di(1H-indol-3-yl)-1,4-dimethylpiperazine-2,5-dione (bisindole piperazine) (Figure 10) and 1,4-dimethyl-3,6-bis[(7H-purin-6-yl) amino] piperazine-2,5-dione (bisadenine piperazine) (Figure 11). The dragmacidin analogs synthesized share a common piperazine center but differ with regards to their indole groups. As the two compounds synthesized are insoluble in aqueous solutions, so are ideal drug compounds for drug-loading with mPEG-PAE.

3.3 Rilpivirine Hydrochloride

Rilpivirine Hydrochloride, 4-[[4-(2-Cyanoethenyl)-2,6-dimethylphenyl) amino]-2-pyrimidinly] amino] benzonitrile monohydrochloride (Figure 12), is a potent non-nucleoside reverse transcriptase inhibitor (NNRTI) from the same chemical class as dapivirine, an approved therapy used to treat HIV-1 infections[41, 42]. Rilpivirine is a pharmaceutical drug that is used as a hydrochloride salt in anti-HIV formulations. The antiviral properties of rilpivirine hydrochloride have brought attention to the possible use of the drug with regards to other viral pathogens. However, the NNRTI drug has a poor solubility and dissolution rate that leads to low bioavailability of the drug[43]. The high prospects as an antiviral drug along with the hydrophobic nature, enforce rilpivirine chloride's potential for the drug-carrier mPEG-PAE.

CHAPTER 4

DRUG-LOADING OF POLYMERIC MICELLES

4.1 Introduction to Drug-Loading of Polymeric Micelles

Advancements in nanomedicine have emerged as a potential solution for the various issues currently inhibiting drug delivery. Biodegradable polymeric nanoparticles play a crucial role in the drug delivery process by optimizing the drug formulation[32]. Polymeric nanocarriers are not only capable of forming stable compounds that are easily degradable but adjustments to their unique properties can increase their specificity for targeted therapy. The polymeric drug carriers described previously are pH-sensitive with diameters of 40-60 nm, close to those of viral pathogens. The pH-specificity of these polymeric micelles assist in retaining their structure thus providing a switching mechanism for the release of drugs at the desired pH.

One of the oldest and most used methods of drug administration via the oral route due to its simplicity, cost-effectiveness, and convenience[44]. Approximately 90% of pharmaceutical products in the global market are administered orally[11]. The yearly market value for these products is estimated to be around $35 billion with an annual growth rate of 10%[9]. However, there are several disadvantages to the oral administration method. The main disadvantages of orally administered drugs are their slow onset of action and the unsuitable use on patients that are unconscious. Factors that affect drug absorption are the poor physicochemical properties of the drug as well as physiological obstacles within the body. Digestive enzymes and stomach acid tend to contribute to the destruction of drugs[32]. Biodegradable polymeric micelles can surpass the limitations of orally administered drugs. The ease of preparation and sterilization, nanosized, and exceptional solubility properties enhance their potential as drug carriers. Most orally administered drugs are absorbed in the upper parts of the gastrointestinal tract and degraded[45, 46]. However, the polymeric micelles act as a protective transportation system enveloping the drug thus shielding it from the harsh physicochemical environment of the GI tract[45, 46]. Furthermore, the tunable properties of the biocompatible polymeric micelles

4.2 Topological Polar Surface Area

A key segment when utilizing polymeric micelles is the determination of the ideal quantity of drug to use. This step is crucial in order to minimize the use of the excess drug when drug-loading polymeric micelles. Along with the cost saving in drugs, there is also a particular phenomenon that has been observed. Along with the decrease in the cost of drug, there is a distinct phenomenon that has been noted to occur. This phenomenon known as multidrug resistance (MDR) is the acquired resistance that microorganisms and cancer cells develop to drugs[7, 8]. MDR has been noted to develop as the result of excess antiviral drugs[47]. MDR occurs because of the overexpression of protein which proceeds to release the antiviral drug from the cell, lowering its concentration and efficiency[47, 48]. Immunosuppressed transplant recipients and patients infected by influenza A virus, hepatitis B virus, and human immunodeficiency virus are

just a few of the of the repercussions of MDR[49]. Therefore, determining the ideal amount for drug-loading is crucial to ensure that the effectiveness of a drug does not decrease.

Polar Surface Area (PSA) is a molecular descriptor that is universally used in the study of drug transportation[50]. PSA operates by utilizing the sum of the surface area on the polar atoms of the molecular structure[50]. PSA has been recognized to correlate well with passive molecular transports within the membranes successfully predicting transport properties of drugs[51]. However, calculating PSA is a time-consuming process due to the need to generate a rational 3D molecular geometry before calculating the surface itself[48]. In 2000, Ertl et al. developed a faster method of calculating PSA through the sum of fragments[47, 48]. Topological Polar Surface Area (TPSA) is defined as the summation of polar atoms fragments within a molecule[48]. A comparison between PSA and TPSA is shown on Figure 13 which notes the simplicity of TPSA. TPSA operates through a compound database that utilizes the polar fragments of a molecule to define its TPSA index[48]. The index allows for faster results equivalent to those of the 3D PSA without the added step[49, 50]. Additionally, the TPSA index of a compound is used in medical chemistry to analyze drug transportation[47, 48]. Compounds with high TPSA are favored as they are more capable for transportation[47, 48]. TPSA can be applied as a method to link two distinct drugs for drug-loading that share a common nanoparticle. The calculated TPSAs are then able to be analyzed to determine the drug loading capability of a novel drug when compared to a more researched drug.

CHAPTER 5

CELL CULTURE BASE SUPPRESSION

5.1 Vero Cell Line

The Vero cells were first derived from the kidney of an African green monkey (*Cercopithecus aethiops*) in 1962 by Yasumura and Kawakita at Chiba University in Japan[52-54]. Since then Vero cells have been used in a number of high-throughput drug screenings (HTDSs)[54]. They are grown on incubation plates where they anchor to the surface of the wells thus forming a monolayer[54]. This method is advantageous due to its simplicity and low maintenance requirements. Additionally, each well represents a different experiment that can be exposed to various concentrations of drugs or viruses. The ease of use of Vero Cells has established them as one of the most used mammalian cell lines with regard to culture, passage, and infection. Figure 14 presents a microscopic image of cultured Vero cells before infection. Vero cells have since contributed to the production of licensed viral vaccines for both inactivated (poliovirus) and live (rotavirus and smallpox) viruses within the United States[52]. Furthermore, Vero cells are currently being used for the drug discovery of various emerging viruses such as Ebola hemorrhagic fever virus, middle eastern respiratory syndrome (MERS) coronavirus, Dengue virus, and Zika virus[52, 53].

There are several advantages when using Vero cell lines for vaccine production. The most common ones are the Vero cells ability to stabilize their genetic traits and their low probability of malignancy[55]. However, Vero cells have two main distinguishing features which differentiate them from other cell lines. Firstly, the Vero cells contain a 9-Mb deletion on chromosome 12, resulting in a type I interferon gene[53, 54]. This particular deletion signifies that the genes will not be able to produce the interferon for alpha or beta[54]. Due to this, Vero cells are more susceptible to viral infections and are commonly used in a number of viral studies including arboviruses such as flaviviruses. Secondly, Vero cell line are continuous[53]. The continuous cell lines fast growth rate has been noted as a valuable resource for vaccine production[56]. Due to the cell lines susceptibility to viral infections and continuous nature, Vero cells are widely used for the study and production of viral vaccines[52].

5.2 Dose Dependence Assay

An essential step in the drug development process is the assessment of a cell's response to the drug. One of the most prevalent techniques used is the dose dependence assay. The dose dependence assay is traditionally performed by exposing cultured cells to prospective drugs in order to evaluate its efficacy and potency[57]. The outcome of these assessments are dependent on the range of concentration and cells used[58]. There are two traditional methods used for the evaluation of a dose-response to a drug, the half-maximal effective concentration (EF50) and the half-maximal inhibitory concentration (IC50)[59]. The 50% effective concentration (EC50) is the assessment of the potency of a drug that induces a biological response halfway between the

baseline and maximum response with an upward curve[60]. EC50 has been noted to be influenced by a drug's affinity and efficacy[60]. The 50% inhibitory concentration (IC50) is the assessment of the potency of a drug that elicits a response midway between the maximum response and the minimum response with a downward slope[60]. Researchers often use IC50 in the pharmaceutical field when determining the potency of a drug with regards to a specific cell line[57]. IC50 indicates the amount of drug needed to inhibit a biological process by 50%[60]. The results may vary depending on the concentration range and cell/tissue type being used[60].

5.3 Plaque Assay

In 1952, the Italian scientist Renato Dulbecco developed a novel technique for animal viruses that had not been developed before which he named the Plaque Assay[61, 62]. Previous to this time, early bacteriologist of the 1920's had used plaque assay to determine the quantity of infectious bacteriophages[63]. Dulbecco noted its potential use in animal virology and modified the procedure during the advancement in cell culture after the release of the HeLa cells[63, 64]. The plaque assay is a standard technique used to determine the virus concentration quantity as it relates to infectious dose[64, 65]. Cultured cells that are susceptible to virus infection are essential when conducting plaque assays within a controlled environment[62]. The assay is based on the quantification of plaque-forming units (PFU) in a monolayer of virus-infected cells[65]. The formation of plaques occurs when an infected cell lyses[65]. Afterward, the surrounding cells undergo the cycle of infection and lysis creating a hole in the monolayer known as a plaque[62, 65]. These plaques are allowed to grow until they become visible to the naked eye at which point they are dyed to enhance the contrast[62, 65]. Ultra violet is often used as it stains cells purple while plaques remain clear due to lacking cells[65].

CHAPTER 6

MATERIALS & METHODS

6.1 Experiment of Diblock polymer, mPEG-PAE

Materials of acrylate mPEG synthesis

Monomethoxy poly (ethylene glycol) (MPEG) (M_n: 5000 Da) CAS # 9004-74-4, Triethylamine (TEA) CAS# 121-44-8, acryloyl chloride CAS# 814-68-6, dichloromethane (DCM) CAS# 75-09-2, Hexane CAS# 110-54-3. All were purchased from Sigma-Aldrich and used as received.

Materials of mPEG-PAE synthesis

The additional materials required for the mPEG-PAE polymerization were: 4,4'-trimethylenedipiperidine (TDP) CAS# 16898-52-5, Hexane-1,6-dioldiacrylate (HDD) CAS# 13048-33-4, chloroform CAS# 67-66-3. All were purchased from Alfa Aesar and used as received.

Synthesis of acrylate mPEG production

Poly (ethylene glycol) methyl ether acrylate (mPEG-A) was obtained by acrylating mPEG with acryloyl chloride. A quantity of 0.2763 g/ mL of monomethoxy poly (ethylene glycol) (mPEG) (1 equiv.) was dissolved in 1mL/ L anhydrous dichloromethane (DCM) at 10% solids concentration in a two-neck round bottom flask in N_2 atmosphere[29]. The catalyst, 278.8 µL/mL triethylamine (TEA), (2 equiv.), was added and cooled in an ice bath at 0 C°. Once the desired temperature was reached, 121.9 µL/mL acryloyl chloride (1.5 equiv.) was added through dropwise addition and allowed to stir at 0 C° for 2 hours. Afterwards, the reaction was brought to room temperature and continued to stir for 24 hours. The reaction was extracted with dilute HCl (1:0.5, v/v) and precipitated with chilled hexane and lyophilized for 48 hours to obtain poly (ethylene glycol) methyl ether acrylate (mPEG-A).

Synthesis of mPEG- poly (β-amino ester) Block Copolymer

The methyl (polyethylene glycol)-Poly (β-amino ester) (mPEG-PAE) copolymer was synthesized via a Michael-type step polymerization using poly (ethylene glycol) methyl ether acrylate (MPEG-A), 4,4'-trimethylenedipiperidine (TDP), and hexane-1,6-dioldiacrylate (HDD). In an N_2 atmosphere setup, 2.2403 mL/ L of HDD (0.01 equiv.) and 2.3149 g/mL of 4,4'-trimethylenedipiperidine (TDP) (0.01 equiv.) were dissolved in 10 mL/ L of chloroform and combined to form poly (β-amino ester) (PAE). The mPEG-A was dissolved in chloroform and combined with the PAE solution and allowed to polymerize for ~48 hours at 50 ℃. The final product was precipitated with chilled diethyl ether and allowed to precipitate for 24 hours in the Boekel Scientific gravity convection digital incubator at 47 ºC. The solid was suspended in double-distilled water and dialyzed (molecular weight cutoff 8 kDa) for 24 hours. The resulting

polymer samples were flash-frozen in liquid nitrogen and lyophilized for 48 hours before being stored at -20 ℃ until further use or characterization.

6.2 Experiment of mPEG-PAE Micelles

The AB diblock polymer, consisting of mPEG-PAE, was utilized to form a blank micelle within a vacant core. Synthesis of the blank micelle was initiated by dissolving the lyophilized mPEG-PAE diblock polymer in ultrapure deionized water (18.2 MW.cm at 25℃) at a ratio of 30 mg polymer per 1 mL of water. Self-assembly of the micelles was thermally-induced by placing the polymer/ ultrapure water solution in a water bath (Thermo Scientific Precision CIR 19) at 50℃ for 15 minutes. Once self-assembly was completed, the solution was filtered through a 0.2 µm syringe filter (Corning sterile syringe filter part no. 431215) The filtrated blank micelles were then characterized using UV-Visual spectroscopy (Shimadzu UV-2600 UV-VIS Spectrophotometer) and dynamic light scattering (Malvern Nano series NANO-ZS ZetaSizer).

6.3 Experiment of Antiviral drug Rilpivirine Hydrochloride

Materials

The synthesis of rilpivirine hydrochloride were (E)-3-(4-amino-3,5-dimethyl phenyl)-2-propenenitrile hydrochloride CAS # 661489-23-2, 4-[(4-chloro-2-pyrimidinyl)-amino] benzonitrile CAS #: 244768-32-9, Acetonitrile CAS #: 75-05-8, Sodium Carbonate CAS #: 497-19-8, Dimethyl Sulfoxide CAS #: 67-68-5

Synthesis of Rilpivirine Hydrochloride

In an N_2 atmosphere setup, 0.0895 g/ mL of 4-[(4-chloro-2-pyrimidinyl)-amino] benzonitrile (4.3 mmol) was combined with 0.0818 g/ mL of (E)-3-(4-amino-3,5-dimethyl phenyl)-2-propenenitrile hydrochloride (4.4 mmol) in 1.000 mL/ L of acetonitrile. The solution was allowed to stir/ reflux at a range of 85-90℃ until completion. The reaction was cooled to ~40℃ and calibrated to pH 10 via dropwise addition of 1.002 g/ mL sodium carbonate solution while recording the pH. The solution was chilled to a range of 5-10℃ and vacuum filtrated with a medium flow filter.

The product was oven dried for 24 hours to yield ~1.1g/ mL of rilpivirine. The rilpivirine was dissolved in an Erlenmeyer flask with acetone and allowed to stir at ~70℃ while adding enough decolorizing charcoal until a grey color appeared. Once the solution was concentrated to ~5mL, the solution was chilled to ~5-10℃ and vacuum filtrated with a medium flow filter. The product was oven dried for 24 hours to yield ~0.8g/ mL of rilpivirine. The rilpivirine was dissolved with 302.5 µL/ mL of dimethyl sulfoxide and heated to a range of 70-75℃. The mixture was cooled to a range of 50-55℃, 250 µL/ mL of hydrochloric acid was added while stirring. The solution was cooled to a range of 40-45℃ and diluted with ultra-pure DI water. Once the solution reached a temperature range of 25-30℃, the solution was vacuum filtrated

with a medium flow filter and oven dried for 24 hours to yield ~0.9g/mL of rilpivirine hydrochloride with $<0.1\%$ z-isomer.

6.4 Experiment of 3,6-di(1H-indol-3-yl)-1,4-dimethylpiperazine-2,5-dione (bisindole piperazine)

Materials

The synthesis of Bisindole was Sarcosine anhydride (1,4-dimethylpiperazine-2,5-dione) CAS #:5076-82-4 Purchased from Fuji Film, Bromine (Br_2) CAS #: 7726-95-6 Purchased from Thermo Scientific, Ortho-dichlorobenzene (ODCB) CAS #: 95-50-1 Purchased from Fisher Scientific, Indole CAS #: 120-72-9 Purchased from Fisher Scientific, Dimethylformamide (DMF) CAS #: 68-12-2 Purchased from Fisher Scientific.

Synthesis of Bisindole Derivative

In an N_2 atmosphere setup, 1.2507 g/ mL sarcosine anhydride (1,4-dimethylpiperazine-2,5-dione) (1 equiv.) was dissolved in 5mL/ L of ortho-dichlorobenzene (ODCB) in a two-neck round-bottomed flask and allowed to stir at a temperature of 150℃ [66, 67]. In a separate Erlenmeyer flask, 1.0 mL/ L of Br_2 (2.2 equiv.) was added to 2.0 mL/ L of ODCB. Once the sarcosine anhydride/ ODCB solution reached 150℃, the Br_2/ ODCB solution was added. The solution then continued to stir at a constant temperature of 150℃ in an N_2 atmosphere under UV lighting for 1 hour. The solution was allowed to cool to room temperature. Afterward, 2.1669 g/ mL of indole (2.1 equiv) was dissolved in 30 mL/ L of DMF. Cooled hexanes were added to solution, filtered, and collected. The brown solid was added to the indole solution and allowed to stir at room temperature under UV lighting for 24 hours. The solution was vacuum filtered with methanol. The melting point and FTIR were analyzed for confirmation of the final product.

6.5 Experiment of 1,4-dimethyl-3,6-bis[(7H-purin-6-yl)amino]piperazine-2,5-dione (bisadenine piperazine)

Materials

The synthesis of Bisadenine with sarcosine anhydride (1,4-dimethylpiperazine-2,5-dione) CAS #:5076-82-4 purchased from Fuji Film, Bromine (Br_2) CAS #: 7726-95-6 Purchased from Thermo Scientific, Ortho-dichlorobenzene (ODCB) CAS #: 95-50-1 Purchased from Fisher Scientific, Indole CAS #: 120-72-9 Purchased from Fisher Scientific, Dimethylformamide (DMF) CAS #: 68-12-2 Purchased from Fisher Scientific, Adenine CAS# 73-24-5 Purchased from Acros Organic.

Synthesis of Bisadenine Derivative

In an N_2 atmosphere setup, 1.2517 g/ mL of sarcosine anhydride (1,4-dimethylpiperazine-2,5-dione) (1 equiv.) was dissolved with 5mL/ L of ortho-dichlorobenzene (ODCB) [66, 67]. In a separate Erlenmeyer flask, 1.0 mL/ L of Br_2 (2.2 equiv.) was combined with 2.0 mL/ L of

ODCB and added dropwise to the sarcosine anhydride/ ODCB mixture at a constant temperature of 150℃ for 1 hour under UV lighting. In a separate Erlenmeyer flask, 2.5042 g/ mL of adenine (2.1 equiv.) was dissolved in 30 mL/ L of DMF and added to the mixture and stirred. Cooled hexanes were added to solution, filtered, and collected. The product was vacuum filtrated with menthol and the final product was collected and analyzed with FTIR and melting point to confirm the product.

6.6 Drug-loading mPEG-PAE Micelles

The quantity of rilpivirine hydrochloride required to thoroughly drug-load the blank micelle sample was determined using topological polar surface area (TPSA) as described in Chapter 4, section 2. The rilpivirine hydrochloride's TPSA can be calculated and compared to drug loaded capacity of a known drug, ribavirin using the formula previously discussed in Chapter 4.

CHAPTER 7

DATA & RESULTS

7.1 Characterization of Diblock, mPEG-PAE

The diblock polymer, mPEG-PAE, was synthesized with the method described in the Methods section. Once the synthesized product was completed, a Fourier transform infrared spectroscopy (FTIR) was performed. The FTIR was performed at the key points of the synthesis as noted on Figure 15. These key points are composed of the mPEG before synthesis, the acrylate mPEG intermediate, and the final mPEG-PAE product after synthesis. The addition of the peak around 1700 cm-1 in the diblock intermediate and final polymer product indicates the presence of the esters from the acrylate mPEG and the PAE segment. The peak around 2900 cm-1 is attributed to C-H stretching found in the mPEG segments. The small peak in the fingerprint region at 1100 cm-1 is the C-O bond from the ether stretching.

7.2 Characterization of Antiviral drug Bisindole Derivative

The synthesis of the Bisindole derivative drug was confirmed through FTIR characterization. The FTIR spectrum of Bisindole had a C=O peak at 1650 cm^{-1}, C-C aromatic peak at 1603 cm^{-1}, and a N-H peak at 3250 cm^{-1} (Figure 16). The melting point of the product was greater than 250 C° with a yield of 22.3%.

7.3 Characterization of Antiviral drug Bisadenine Derivative

The synthesis of the Bisadenine derivative drug was confirmed through FTIR characterization. The FTIR spectrum of Bisadenine had an elongation N-H stretch at 3250 cm^{-1}, C=O stretch at 1658 cm^{-1}, and an elongated aromatic C-C stretch at 1603 cm^{-1} (Figure 17). The melting point of the product was greater than 250 C° with a final yield of 38.5%.

7.4 Characterization of Bisadenine-Loaded mPEG-PAE Micelles

The drug-loaded diblock micelle was composed of the mPEG-PAE thermo-induced micelles and the synthesized bisadenine drug. The term “blank” refers to the micelles that have recently been synthesized and characterized to ensure the micelle formation without the addition of drug. The term “loaded” refers to a micelle that has been sonicated and characterized with the addition of drug. The loaded mPEG-PAE micelle is approximately around 310nm and has an increase in absorbance while the blank mPEG-PAE micelle is red shifted to approximately 220nm (Figure 18). The Bisadenine derivative drug alone can be noted at a peak of around 310nm.

The bisadenine-loaded micelles were characterized further to ensure that the status of the micelles was adequate. The micellar surface charge of the drug-loaded micelles was analyzed through the zeta potential and dynamic light scattering. Dynamic light scattering calculates the

average diameter per micelle particle in suspension. These steps are essential to predict major repulsive or attractive forces within the drug-loaded micelle that may become a reason for concern during *in vitro* analysis. The zeta potential of the bisadenine-loaded mPEG-PAE micelles was 7.91 $\pm$ 4.98 mV (Figure 19) and the average diameter of the micelles were 165.31 $\pm$ 17.61 nm with a PDI of 0.545 (Figure 20). By ensuring that the surface charge of the drug-loaded micelles is within ±30 mV, the micelles should not experience any attractive or repulsive forces when tested *in vitro*. This should ensure that the micelles do not aggregate and be capable of entering the cells without any issues.

7.5 Characterization of Bisindole-Loaded mPEG-PAE Micelles

The bisindole-loaded micelles were synthesized and characterized in a similar fashion as the bisadenine-loaded micelles. UV-VIS spectroscopy was used to ensure that the bisindole was loaded into the mPEG-PAE micelle (Figure 21). The Bisindole drug alone was noted to have a main peak at around 200nm with a minor peak at 270nm. Afterwards, the sample was characterized with DLS and zeta potential to measure the micellar surface charge. The zeta potential of the bisindole-loaded mPEG-PAE micelles was 15.5 $\pm$ 6.62 mV (Figure 22). The average diameter of the micelles was 182.4 $\pm$ 16.98 nm with a PDI of 0.521 (Figure 23).

7.6 Characterization of Rilpivirine Hydrochloride

After the mPEG-PAE micelles were drug loaded with rilpivirine hydrochloride, they were characterized using UV-VIS spectroscopy to ensure the loading of the micelles when compared to the blank mPEG-PAE micelles (Figure 24). The average diameter of the micelles was determined to be 165.3 $\pm$ 17.61 nm (Figure 25).

CHAPTER 8

DISCUSSION

The goal for designing and producing biodegradable polymeric micelles were for their overall benefits with regards to the safety and effectiveness that they display as drug-carriers. The broad range of features of polymeric micelles has attracted attention due to the endless list of possible applications. Currently, most of the research on polymeric micelles is being obtained for drug-delivery in the cancer field. However, the similarities shared by cancer cells and viruses have connected a possible opportunity of using polymeric micelles for the ongoing battle against viruses. Unlike various other drug-delivery systems available today, AB diblock polymeric micelles are composed of a single layer of lipid which facilitates the effectiveness of dissociation of the diblock polymeric micelles in low acidic environments[31]. The block polymers are also capable of adjusting to different environments for drug delivery depending on the composition of each segment.

The amphiphilic copolymer micelle was synthesized through two syntheses. Initially, the mPEG was acrylated and tested to ensure that the synthesis was successful. Afterward, the acrylated mPEG was synthesized through a Michael step polymerization with TDP and HDD which ensured the proper coupling of the A segment to the B segment. Once polymerization was completed, the product was analyzed using the Fourier transform infrared spectroscopy (FTIR) and the peak values were compared to this from the literature values as the mPEG-PAE polymer is not novel.

After the characterization of the mPEG-PAE polymer, the FTIR peaks were compared to literature values to confirm accurate polymerization of the diblock. The addition of the peak around the 1700 cm-1 in the intermediate acrylate mPEG part of the synthesis indicates the presence of an ester. The stretch of the peak continues to elongate once the synthesis was complete due to the additional esters from the PAE segment of the polymer. The peak at approximately 2900 cm-1 where the OH peak is most prominent is attributed to the C-H stretch from the mPEG segment. It can also be concluded that the peak within the fingerprint region at approximately 1100cm-1 is due to the ether stretching from the mPEG segment. After analyzing and comparing the results with literature values, it was determined that the synthesis of mPEG-PAE was complete, and the self-assembly process commenced.

This method ensured the micelles were not suspended in a toxic solvent but rather were suspended in and drug loaded in ultra-pure DI water. Once formed, the blank micelles were checked to ensure micelle formation via UV-vis spectroscopy and dynamic light scattering before moving on to drug loading.

The method used for the micelle formation was beneficial due to the ease in self-assembly as well as the advantage of reducing the use of toxic solvents. The process only required an aqueous solution, ultra-pure DI water was used and placed in a hot bath at the required temperature for self-assembly. Once the blank micelles were formed, they were characterized via UV-Vis spectroscopy and dynamic light scattering to ensure the proper

formation of the micelles. After analysis was complete, the micelles were ready to be drug-loaded.

In order to determine the quantity of drug required to efficiently drug-load the micelles, topological polar surface area (TPSA) was run on the three molecules bisadeninine, bisindole, and rilpivirine hydrochloride. Ribavirin's TPSA was calculated via the software, Molinspiration Cheminformatics

The TPSA of Ribavirin (143.73$Å^2$) was used as a reference drug as the drug loading capacity of a ribavirin-loaded mPEG-PAE micelle was known from previous experiments as well as through literature values. The drug loading capacity of ribavirin is 3.82 mg/mL per 30 mg/mL of mPEG-PAE. The TPSA of bisadenine, bisindole, and rilpivirine hydrochloride were determined through the software, Molinspiration Cheminformatics. The TPSA of bisindole was determined to be 72.20$Å^2$. Using Ribavirin as a reference in the formula in Formula 1, the drug loading capacity of bisindole was determined to be 9.11 mg/mL per 30mg/mL of mPEG-PAE. Once drug-loaded, the micelles were then sonicated for 4 hours and characterized.

The results of the UV-Vis for the drug-loaded micelles displayed positive results as the blank micelles were red shifted and slightly lower in absorbance due to the absence of drug when compared to the drug-loaded results. The zeta potential of the bisadenine-loaded mPEG-PAE micelles was 7.91 $\pm$ 4.98 mV (Figure 19) with an average diameter of the micelles were 165.31 $\pm$ 17.61 nm. As was noted previously, by ensuring that the surface charge of the drug-loaded micelles is within ±30 mV s, the micelles should not experience any attractive or repulsive forces. This should ensure that the micelles do not aggregate and be capable of entering the cells without any issues when tested *in vitro.* The bisadenine and bisindole results for the zeta potential and the average diameter of the micelle were close and although the zeta potential of the rilpivirine hydrochloride was larger than the other two, the stability of the mPEG-PAE micelles remained consistent.

CHAPTER 9

CONCLUSION & FUTURE OUTLOOK

Since the work by Ivanovsky and Beijerinck on the transmission of tobacco mosaic virus demonstrated the existence of an infectious agent capable of surpassing porcelain ultrafilters almost 100 years ago, the field of virology has rapidly grown. The assistance in advancements in technology have furthered our knowledge with regards to viruses and enabled us to search for new methods to combat infectious diseases. Along with the benefits of increasing use of technology comes the possible side effects that may bring risk. The increasing risk in temperature due to global warming has contributed to the increase in risk from mosquito-borne infections. The majority of which are known carriers of viruses from the *Flaviviruses* family and are well-known for their hazardous side-effects to the host that has been bitten. The increase in international travel is also a well-known factor for the spread of various pathogens as was noted during the 2014 Fifa World Cup where natives from French Polynesia are believed to have been the carriers of the Zika virus that led to massive outbreak throughout Brazil and eventually the rest of South and Central America. Due to lack of capable antiviral vaccines and lack of effective mosquito control methods, there is very little that can be done without risking the health of those around. As such, the only possible pathway available would be to improve the antiviral vaccines available which would require improving their capability of fighting off the virus without losing any of the required drug concentration along the way. Due to this the primary objective of this project is aimed at the development of efficient pH-responsive, biodegradable co-polymeric micelles that can improve the efficiency of drug delivery.

By utilizing the preliminary data that supports the successful synthesis and drug loading of the dragmacidin derivatives, 3,6-di(1H-indol-3-yl)-1,4-dimethylpiperazine-2,5-dione (bisindole piperazine) and 1,4-dimethyl-3,6-bis[(7H-purin-6-yl)amino]piperazine-2,5-dione (bisadenine piperazine), and the MPEG-poly(b-amino ester) block copolymer (mPEG-PAE), future works will concentrate on *in vitro* testing of the drug-loaded micellar nanoparticles on cultured cells. Further research will be carried out by testing the drug-loaded mPEG-PAE micelles on other cell lines such as JEG-3 (clonally derived, placenta cancer cells) and BHK (baby hamster kidney fibroblast). Once *in vitro* testing of drug-loaded mPEG-PAE micelles is completed and approved for safe use, the following stages are *in vivo* testing on lab mice to test out the reliability, effectiveness, and safety of the nanoparticle micelles in living mammals infected with Zika virus.

The ability to maintain the potency and effectiveness of current and future vaccines within an infected host may soon be achievable with future research. The potential of developing a stable polymeric micelle capable of containing a diverse range of hydrophobic antiviral drugs without the risk of aggregation is only the beginning. Further experiments will test out the suppression ability of mPEG-PAE through thorough inspection of the loaded and unloaded phases of the micelle. The possibilities of biodegradable polymeric micelles range beyond that of

mPEG-PAE and may lead to further enhancements that may bring about upgraded drug-carriers. Although the current research is still within the initial phases, the positive data thus far has shown encouraging results that can assist in stabilizing the foundation for further research.

LIST OF FIGURES

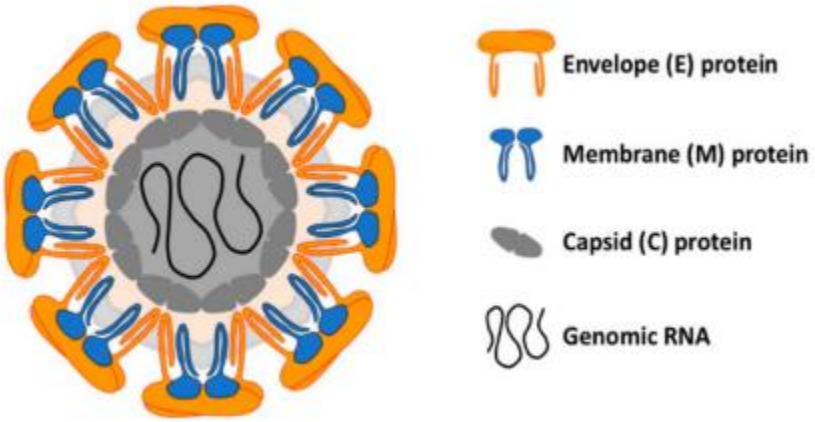

Figure 1. Schematic representation of a mature *Flavivirus* virus exhibiting the outer protein shell enveloping the viral RNA[15].

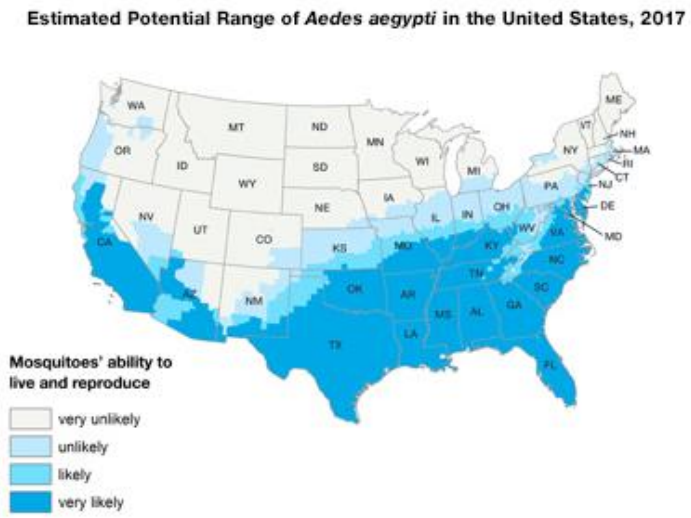

Figure 2. The 2017 CDC estimate of the potential ability of survival and reproduction of *Aedes aegypti* within the United States[19].

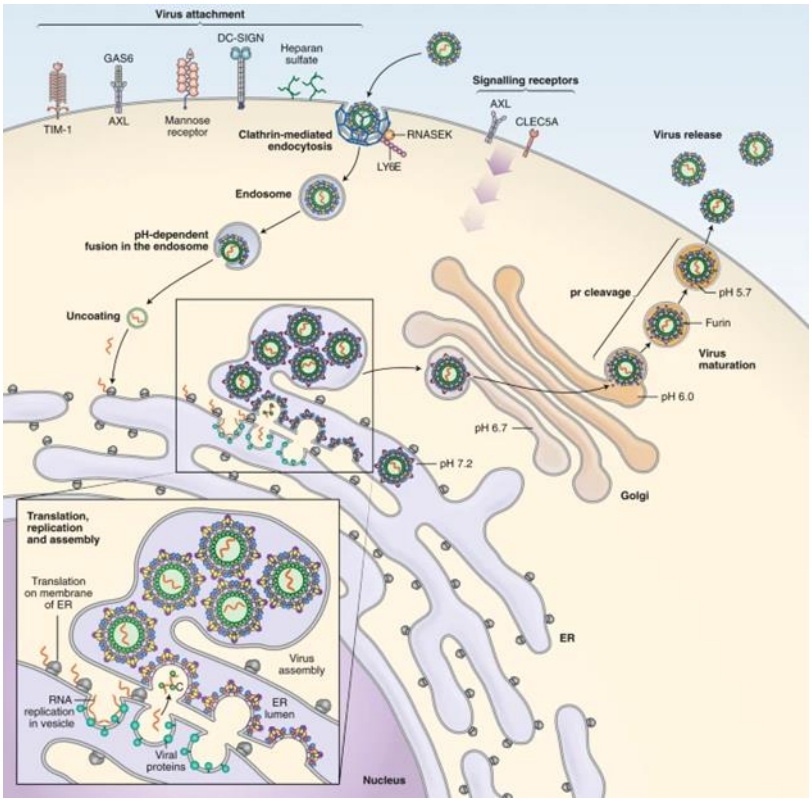

Figure 3. The Zika virus replication life cycle where fundamental steps are determined by distinct pHs[15].

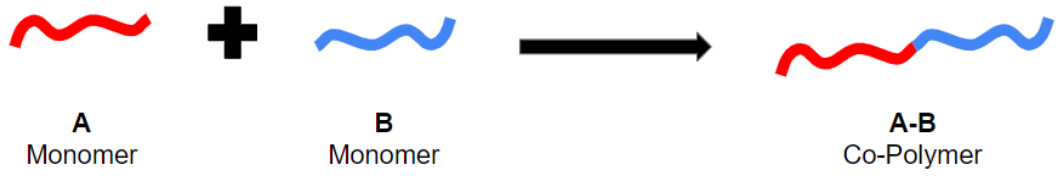

Figure 4. General scheme of an AB diblock formation.

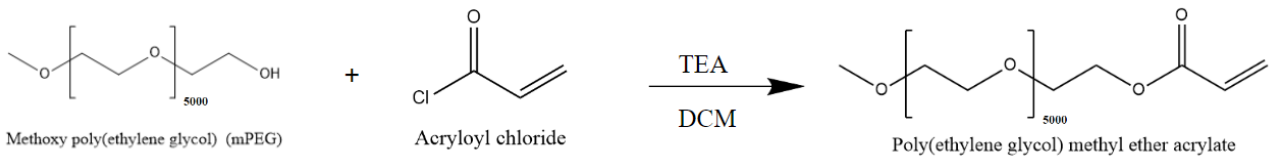

Figure 5. Poly (ethylene glycol) methyl ether acrylate synthesis[29].

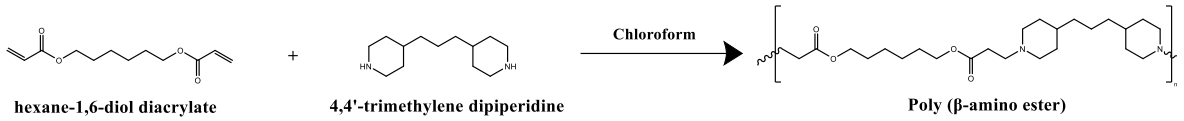

Figure 6. Poly (β-amino ester) synthesis.

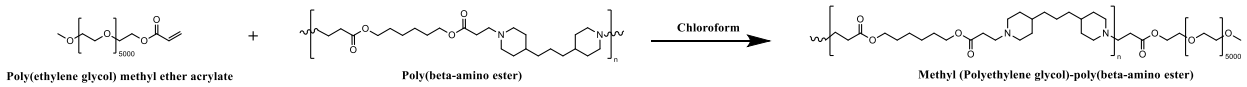

Figure 7. Michael-type step polymerization of mPEG- poly (β-amino ester)[29].

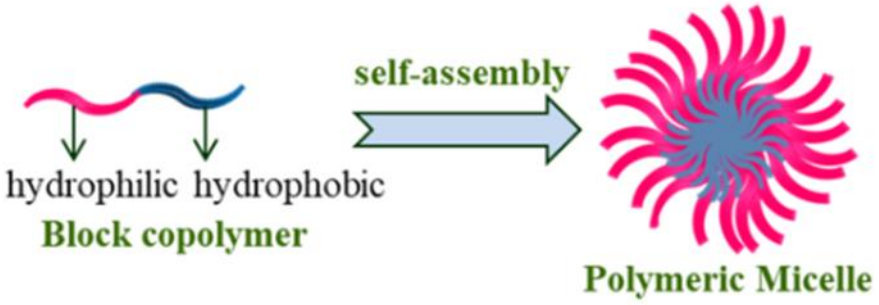

Figure 8. General scheme of the self-assembly process of the AB diblock copolymer[31].

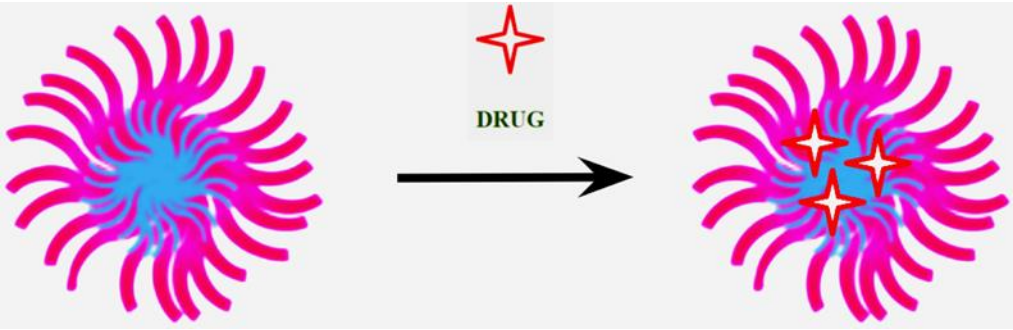

Figure 9. Drug-loading process of the newly formed amphiphilic micelle[31].

Figure 10. The schematic scheme of Bisindole Piperazine[66, 67].

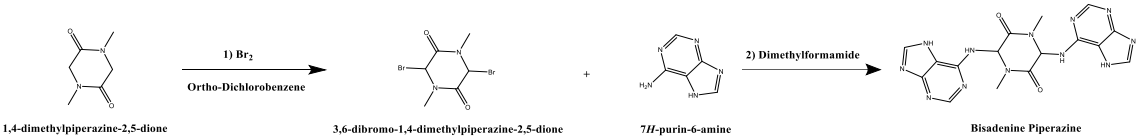

Figure 11. The schematic scheme of Bisadenine Piperazine[66, 67].

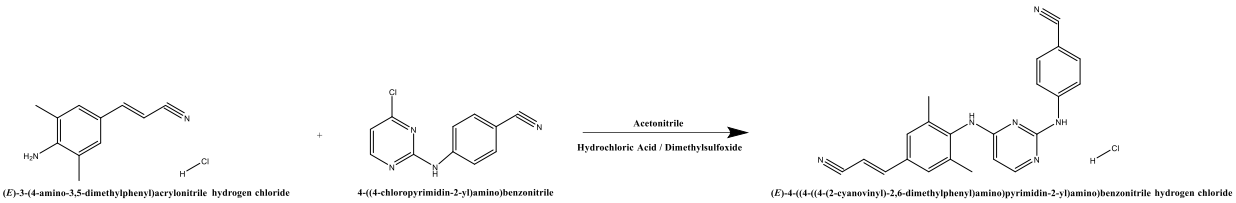

Figure 12. Schematic scheme of Rilpivirine Hydrochloride[42, 43].

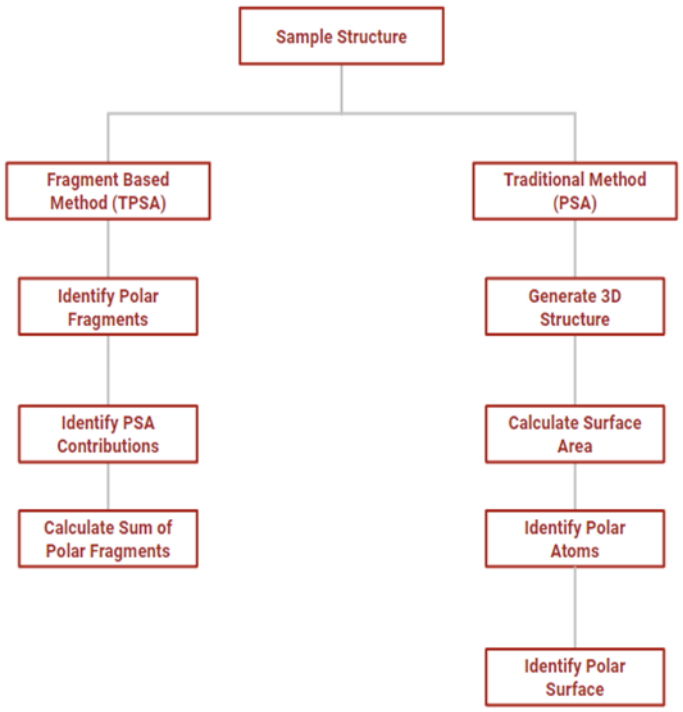

Figure 13. Comparison of the two drug-loading determination methods[48, 51].

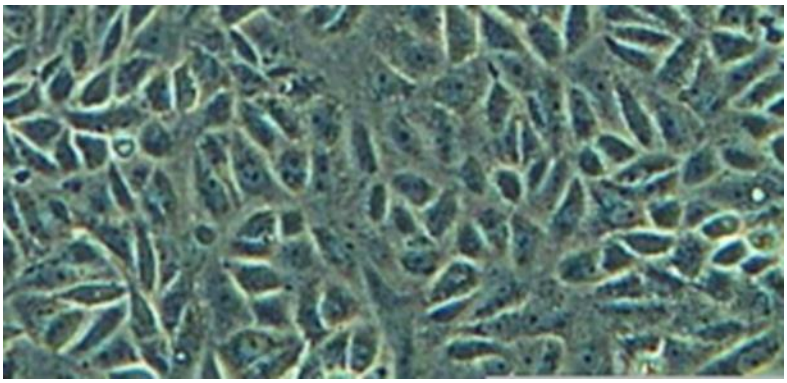

Figure 14. A 200 µm microscopic image of a monolayered Vero cell[68].

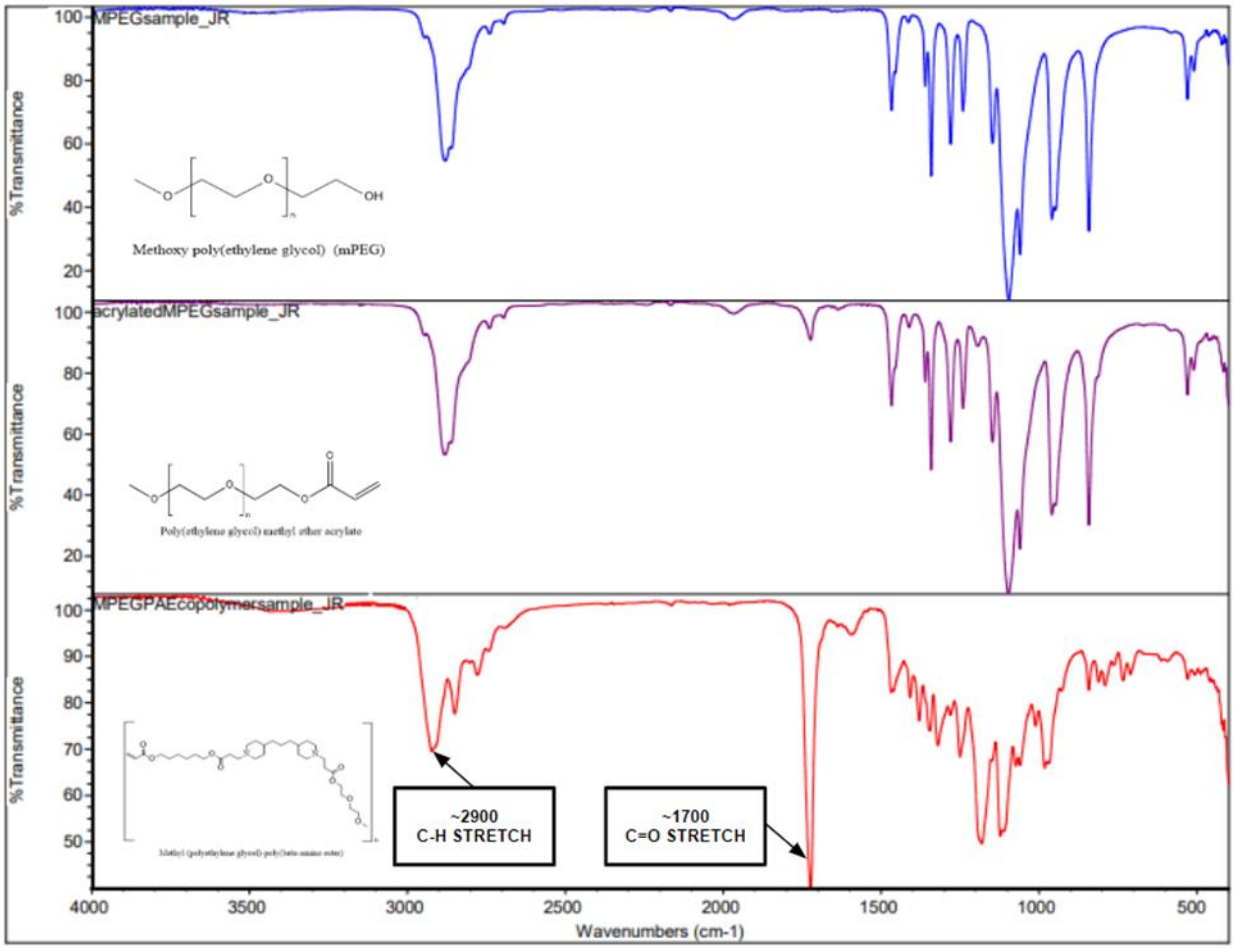

Figure 15. FTIR analysis of mPEG-PAE synthesis at different points of the synthesis.

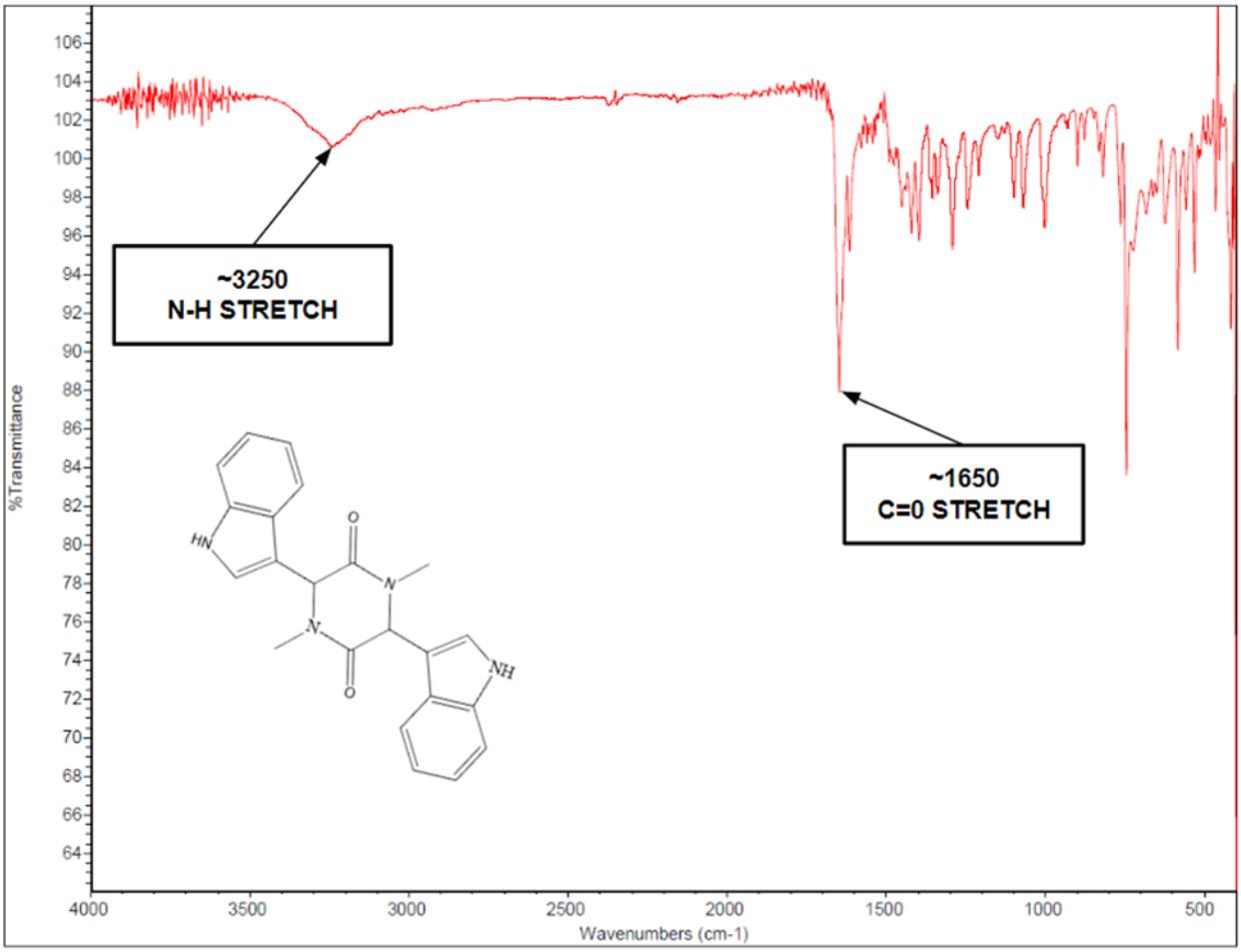

Figure 16. FTIR of the Bisindole Derivative compound.

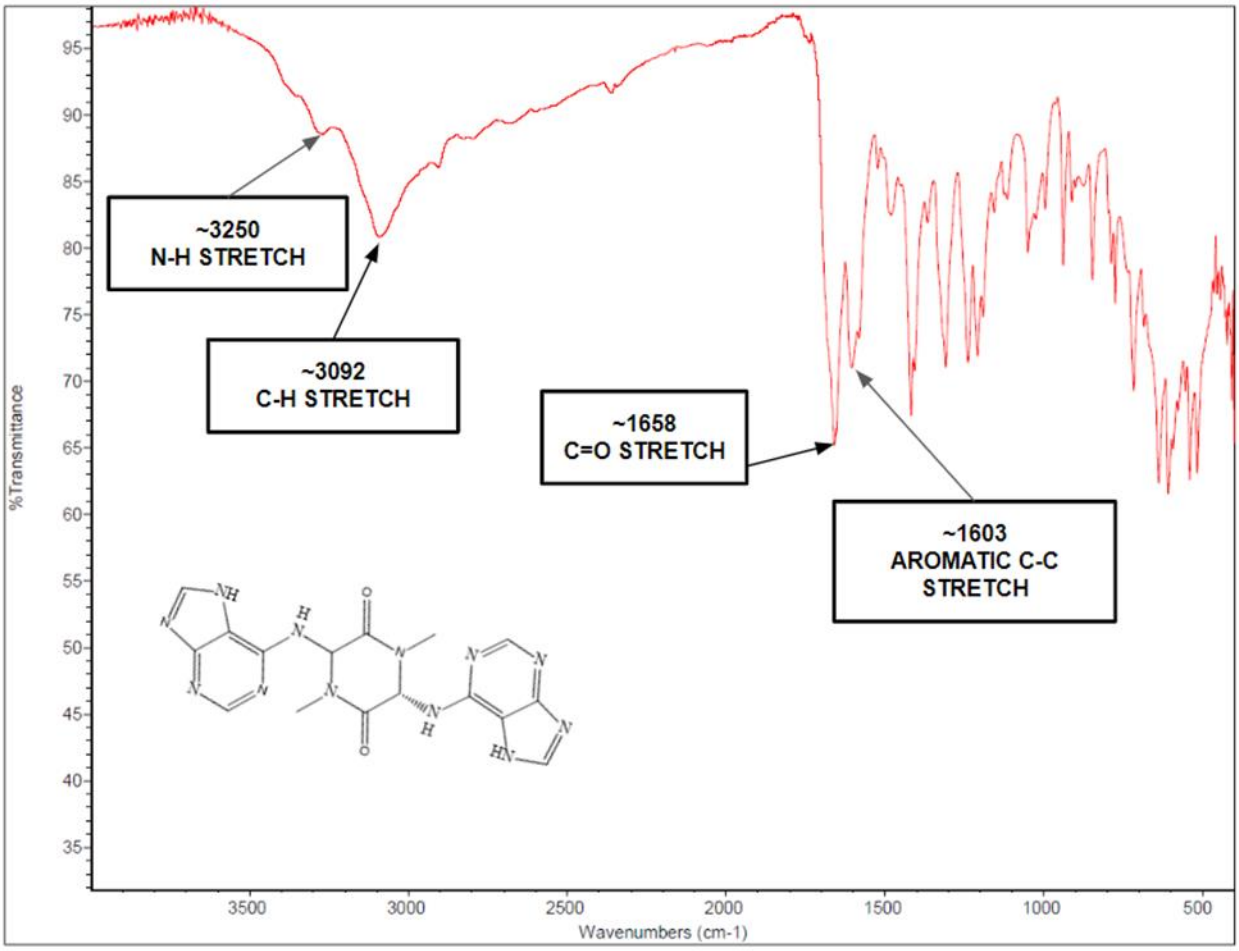

Figure 17. FTIR of the Bisadenine derivative compound.

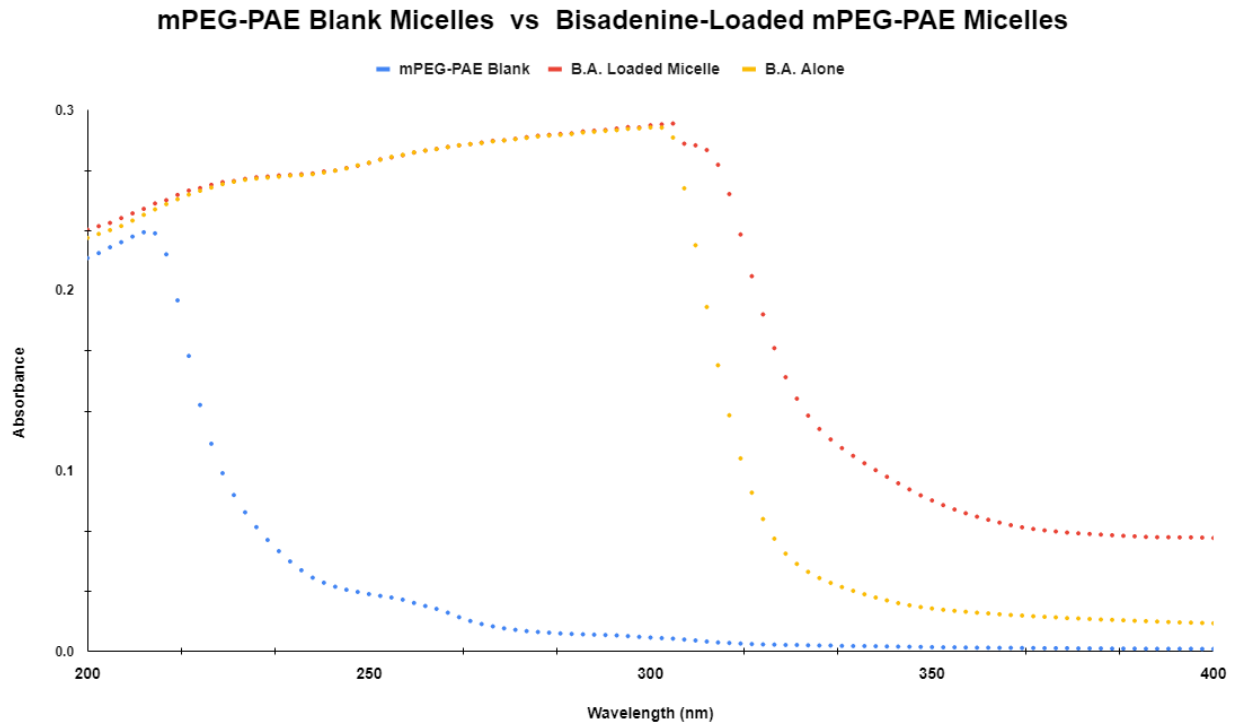

Figure 18. UV-Visual spectroscopy analysis comparing the blank mPEG-PAE micelles with the Bisadenine-Loaded mPEG-PAE in ultra pure DI water.

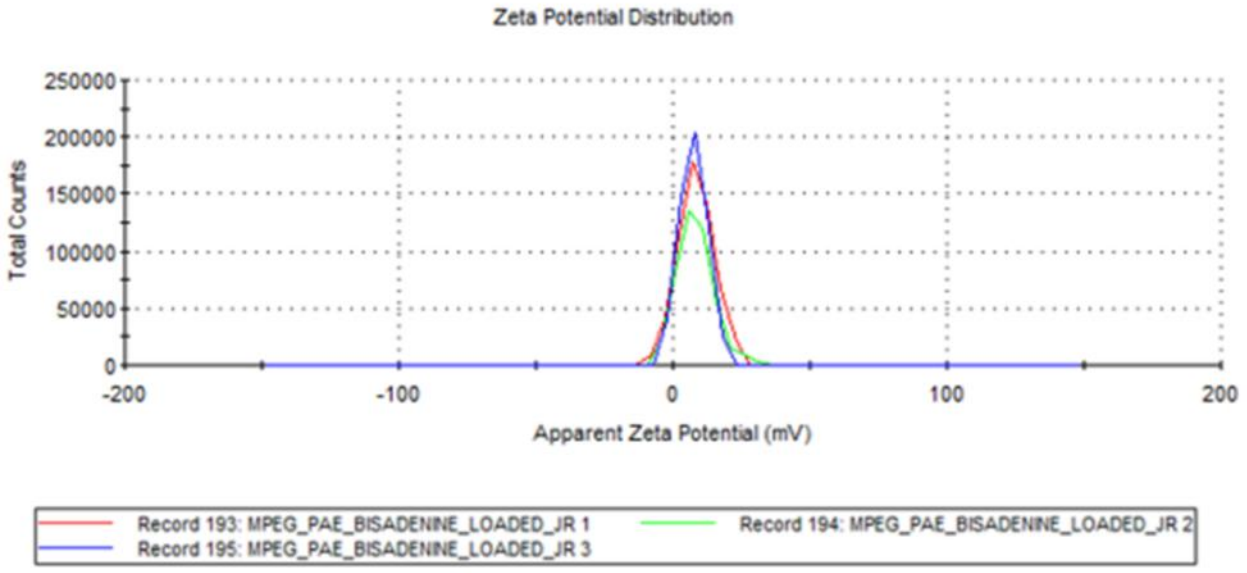

Figure 19. The zeta potential of the bisadenine-loaded mPEG-PAE micelles were suspended in ultra-pure DI water.

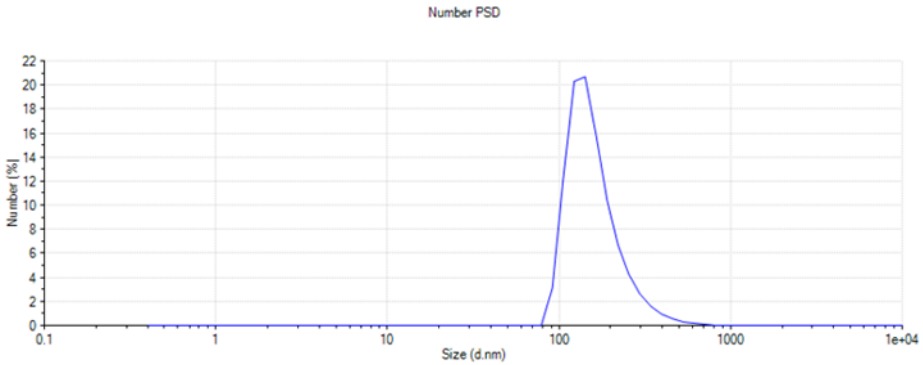

Figure 20. Dynamic Light Scattering was used to determine the average diameter of the Bisadenine-loaded mPEG-PAE micelles that were suspended in ultra-pure DI water.

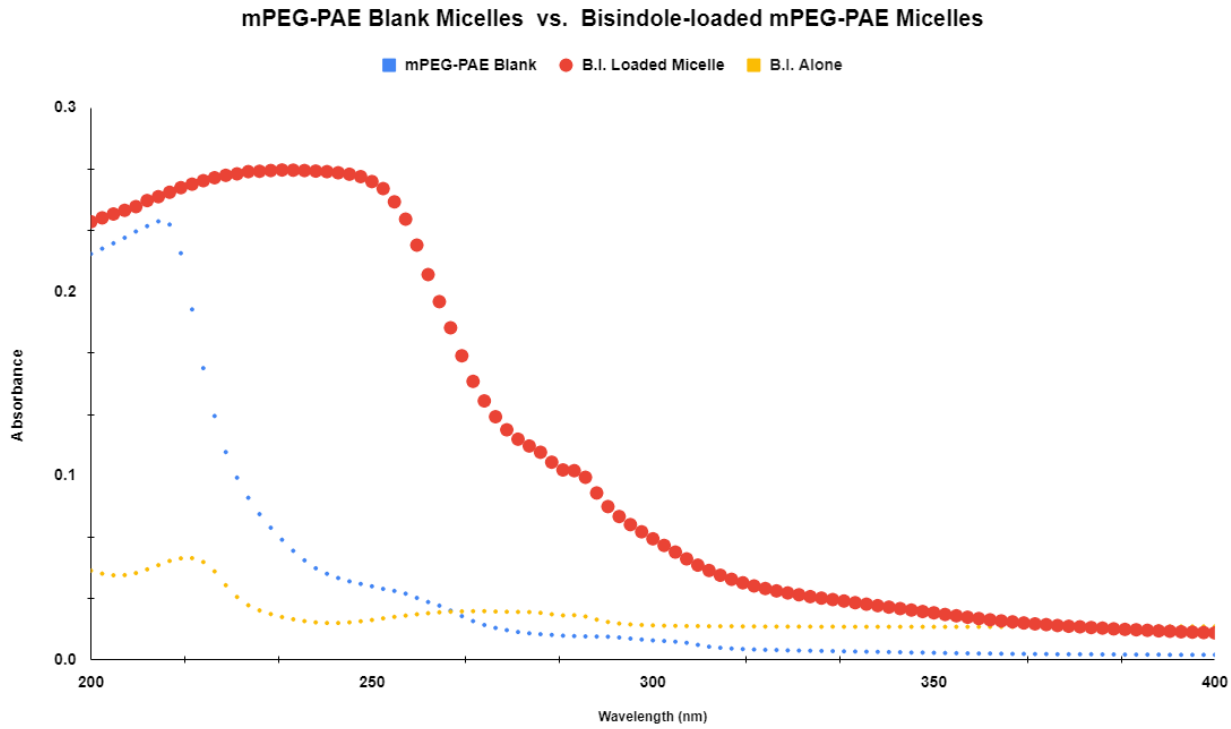

Figure 21. UV-Visual spectroscopy analysis comparing the blank mPEG-PAE micelles with the Bisindole-Loaded mPEG-PAE in ultra-pure DI water.

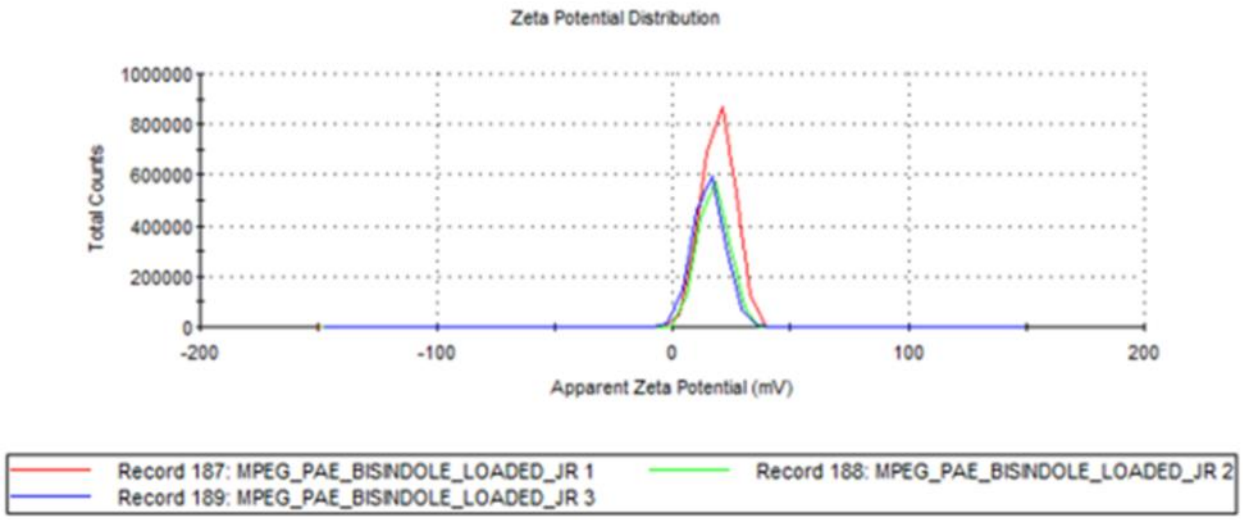

Figure 22. The zeta potential of the bisindole-loaded mPEG-PAE micelles were suspended in ultra-pure DI water.

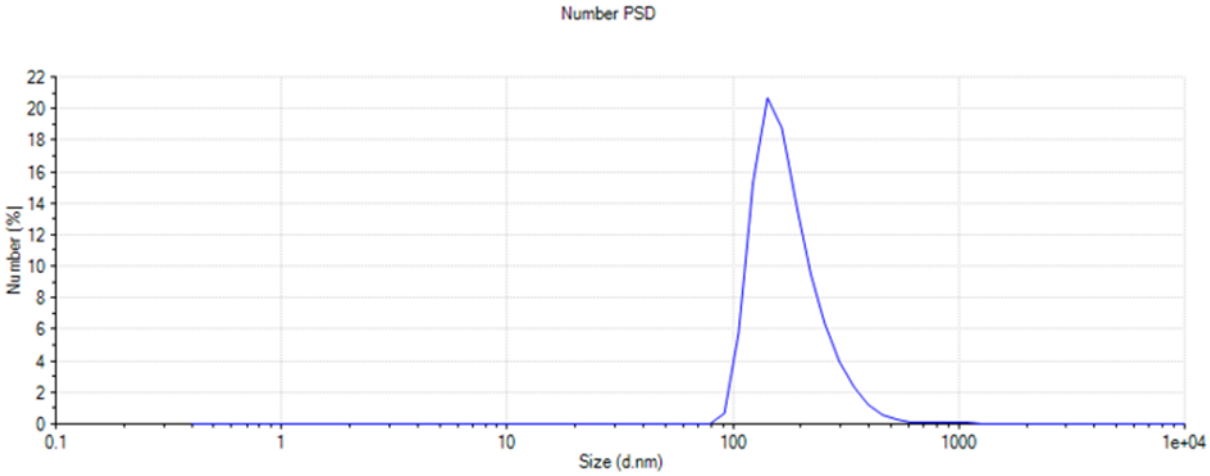

Figure 23. Dynamic Light scattering was used to determine the average diameter of the bisindole-loaded mPEG-PAE micelles that were suspended in ultra-pure DI water.

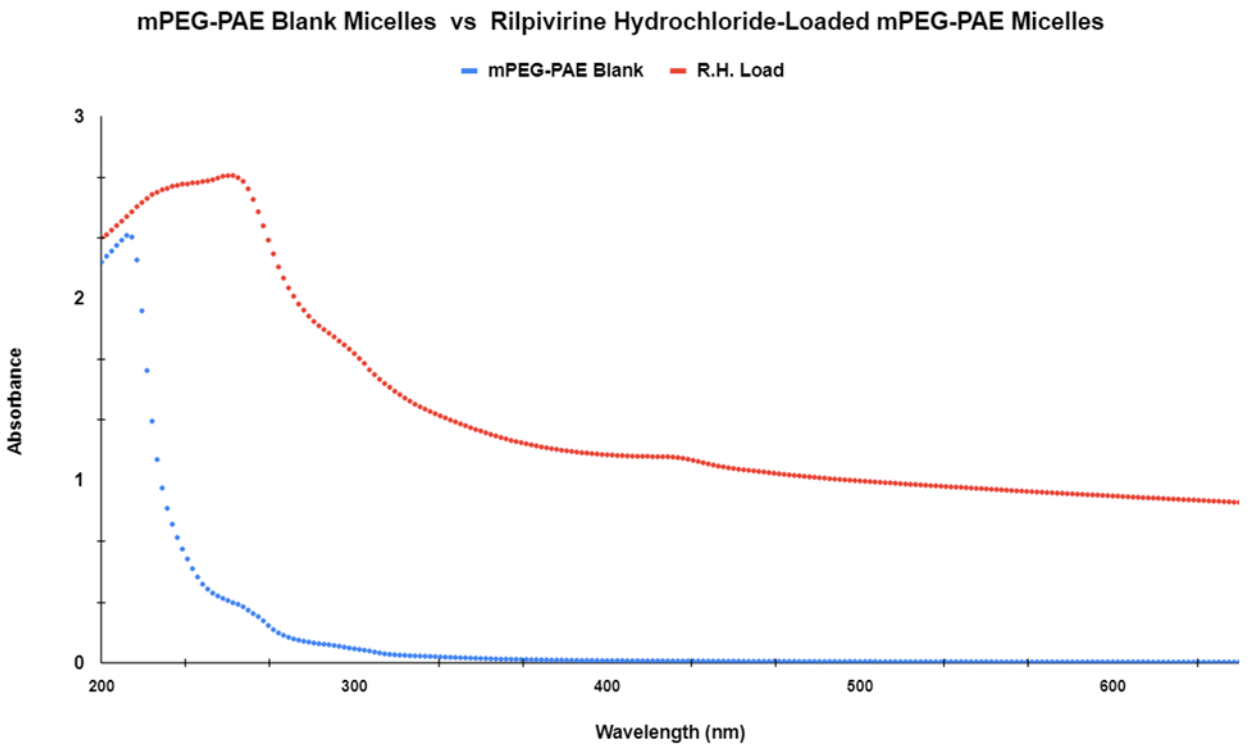

Figure 24. UV-Visual spectroscopy analysis comparing the blank mPEG-PAE micelles with the Rilpivirine Hydrochloride-Loaded mPEG-PAE in ultra-pure DI water.

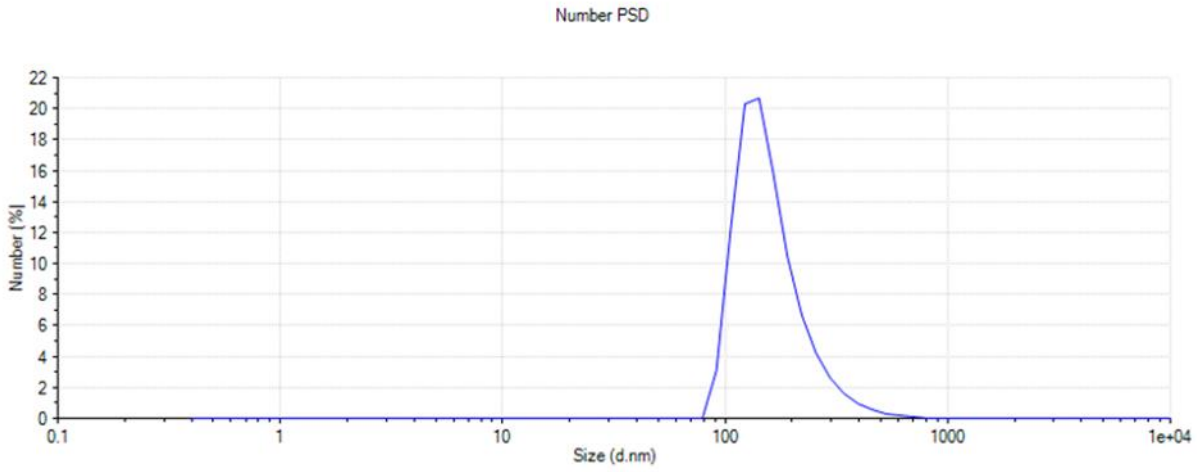

Figure 25. Dynamic Light Scattering (DLS) was used to determine the average diameter of the Rilpivirine Hydrochloride-loaded mPEG-PAE micelles that were suspended in ultra-pure DI water.

LIST OF FORMULAS

$$\frac{(mg\ of\ drug\ known\ to\ load)(TPSA\ of\ drug\ in\ \text{Å}^2)}{(mg\ of\ polymer\ per\ mL\ of\ ultra\ pure\ )} = \frac{(X)(TPSA\ of\ new\ drug\ in\ \text{Å}^2)}{(mg\ of\ polymer\ per\ mL\ of\ ultra\ pure\ )}$$

Formula 1. The drug loading capacity of a drug is determined using the TPSA of a known drug.

LIST OF TABLES

Drugs	TPSA
Ribavirin	143. 73 $Å^2$
Bisindole Piperazine	72.20 $Å^2$
Rilpivirine Hydrochloride	97.42 $Å^2$
Bisadenine Piperazine	173.61 $Å^2$

Table 1. The calculated TPSA for the drugs calculated through the software Molinspiration Cheminformatics.

REFERENCES

(1) Chapter 1 - The Nature of Viruses. In *Fenner's Veterinary Virology (Fifth Edition)*, MacLachlan, N. J., Dubovi, E. J. Eds.; Academic Press, 2017; pp 3-16.
(2) Taylor, M. W. Introduction: A Short History of Virology. From 2014 Jul 22.
(3) Burrell, C. J.; Howard, C. R.; Murphy, F. A. History and Impact of Virology. **2017**, 3-14. DOI:10.1016/B978-0-12-375156-0.00001-1 From 2017.
(4) Taylor; M.W. *What Is a Virus* https://www.ncbi.nlm.nih.gov/pmc/articles/PMC7122971/ (accessed March 17, 2023).
(5) *Viruses*. https://microbiologysociety.org/why-microbiology-matters/what-is-microbiology/viruses.html (accessed March 17, 2023)
(6) *Virus*. https://www.genome.gov/genetics-glossary/Virus (accessed March 15, 2023).
(7) Méthot, P. O. Writing the history of virology in the twentieth century: Discovery, disciplines, and conceptual change. (1879-2499 (Electronic)). From 2016 Oct.
(8) *Virology*. https://www.britannica.com/science/virology (accessed November 10, 2022).
(9) *What are VHF's*. https://www.cdc.gov/vhf/about.html#:~:text=The%20term%20%E2%80%9Cviral%20hemorrhagic%20fever,often%20include%20bleeding%2C%20or%20hemorrhaging (accessed December 12, 2022).
(10) Mangat; R, L. T. *Viral Hemorrhagic Fevers*. StatPearls Publishing, 2023. https://www.ncbi.nlm.nih.gov/books/NBK560717/
(11) Ftika, L.; Maltezou, H. C. Viral haemorrhagic fevers in healthcare settings. (1532-2939 (Electronic)). From 2013 Mar.
(12) Simmonds, P.; Becher, P.; Bukh, J.; Gould, E. A.; Meyers, G.; Monath, T.; Muerhoff, S.; Pletnev, A.; Rico-Hesse, R.; Smith, D. B.; et al. ICTV Virus Taxonomy Profile: Flaviviridae. *Journal of General Virology* **2017**, *98* (1), 2-3. DOI: https://doi.org/10.1099/jgv.0.000672.
(13) Greaves, I.; Hunt, P. Biological Agents. From 2010.
(14) Tomori, O. Yellow fever: the recurring plague. (1040-8363 (Print)). From 2004.
(15) Pierson; T.C.; Diamond, M. S. The continued threat of emerging flaviviruses. Nat. Microbiol. , 2020; Vol. 5, pp 185-192.
(16) *Zika Virus*. https://www.who.int/news-room/fact-sheets/detail/zika-virus (accessed November 15, 2022).
(17) *Life Cycle of Aedes aegypti and Ae. albopictus Mosquitoes*. https://www.cdc.gov/mosquitoes/about/life-cycles/aedes.html# (accessed November 16, 2022).
(18) Powell, J. R.; Tabachnick, W. J. History of domestication and spread of Aedes aegypti--a review. (1678-8060 (Electronic)). From 2013.
(19) *Potential Range of Aedes Mosquitoes*. https://www.cdc.gov/mosquitoes/mosquito-control/professionals/range.html (accessed November 16, 2022).
(20) *Zika*. https://www.who.int/news-room/questions-and-answers/item/zika (accessed November 15, 2022).
(21) Gerold, G. A.-O.; Bruening, J.; Weigel, B.; Pietschmann, T. Protein Interactions during the Flavivirus and Hepacivirus Life Cycle. (1535-9484 (Electronic)). From 2017 Apr.
(22) Marbán-Castro, E.; Goncé, A.; Fumadó, V.; Romero-Acevedo, L.; Bardají, A. Zika virus infection in pregnant women and their children: A review. (1872-7654 (Electronic)). From 2021 Oct.

(23) *Potential Range of Aedes aegypti and Aedes albopictus in the United States, 2017*. https://www.cdc.gov/mosquitoes/mosquito-control/professionals/range.html (accessed November 11, 2022).
(24) Hygino da Cruz, L. C. J. A.-O.; Nascimento, O. A.-O. X.; Lopes, F. A.-O.; da Silva, I. A.-O. Neuroimaging Findings of Zika Virus-Associated Neurologic Complications in Adults. (1936-959X (Electronic)). From 2018 Nov.
(25) Rubin, E. J. a. G. M. F. a. B. L. R. Zika Virus and Microcephaly. *New England Journal of Medicine* **2016**, *374* (10), 984-985. DOI: 10.1056/NEJMe1601862 , note = PMID: 26862812.
(26) *Zika Virus*. https://www.cdc.gov/zika/symptoms/treatment.html#:~:text=There%20is%20no%20specific%20medicine,Drink%20fluids%20to%20prevent%20dehydration (accessed February 17, 2023).
(27) Nathanson, N. Chapter 1 - The Human Toll of Viral Diseases: Past Plagues and Pending Pandemics. In *Viral Pathogenesis (Third Edition)*, Katze, M. G., Korth, M. J., Law, G. L., Nathanson, N. Eds.; Academic Press, 2016; pp 3-16.
(28) Craig; E. *Chapter 7-Applications of Nanoparticles*; Larsen and Keller Education, 2019.
(29) Kim, M. S.; Hwang, S. J.; Han, J. K.; Choi, E. K.; Park, H. J.; Kim, J. S.; Lee, D. S. pH-Responsive PEG-Poly(β-amino ester) Block Copolymer Micelles with a Sharp Transition. *Macromolecular Rapid Communications* **2006**, *27* (6), 447-451, https://doi.org/10.1002/marc.200500769. DOI: https://doi.org/10.1002/marc.200500769 (acccessed 2023/05/04).
(30) Craig; E. *Chapter 1-Introduction to Nanomaterials*; Larsen and Keller Education, 2019.
(31) Kuperkar, K.; Patel, D.; Atanase, L. I.; Bahadur, P. Amphiphilic Block Copolymers: Their Structures, and Self-Assembly to Polymeric Micelles and Polymersomes as Drug Delivery Vehicles. In *Polymers*, 2022; Vol. 14.
(32) Ghezzi, M.; Pescina, S.; Padula, C.; Santi, P.; Del Favero, E.; Cantù, L.; Nicoli, S. Polymeric micelles in drug delivery: An insight of the techniques for their characterization and assessment in biorelevant conditions. (1873-4995 (Electronic)). From 2021 Apr 10.
(33) Li, W.; Zhan, P.; De Clercq, E.; Lou, H.; Liu, X. Current drug research on PEGylation with small molecular agents. *Progress in Polymer Science* **2013**, *38* (3), 421-444. DOI: https://doi.org/10.1016/j.progpolymsci.2012.07.006.
(34) Iqbal, S.; Qu, Y.; Dong, Z.; Zhao, J.; Rauf Khan, A.; Rehman, S.; Zhao, Z. Poly (β-amino esters) based potential drug delivery and targeting polymer; an overview and perspectives (review). *European Polymer Journal* **2020**, *141*, 110097. DOI: https://doi.org/10.1016/j.eurpolymj.2020.110097.
(35) Das, S. S.; Bharadwaj, P.; Bilal, M.; Barani, M.; Rahdar, A.; Taboada, P.; Bungau, S.; Kyzas, G. Z. Stimuli-Responsive Polymeric Nanocarriers for Drug Delivery, Imaging, and Theragnosis. In *Polymers*, 2020; Vol. 12.
(36) De Clercq, E.; Li, G. Approved Antiviral Drugs over the Past 50 Years. (1098-6618 (Electronic)). From 2016 Jul.
(37) Bryan-Marrugo, O. L.; Ramos-Jiménez, J.; Barrera-Saldaña, H.; Rojas-Martínez, A.; Vidaltamayo, R.; Rivas-Estilla, A. M. History and progress of antiviral drugs: From acyclovir to direct-acting antiviral agents (DAAs) for Hepatitis C. *Medicina Universitaria* **2015**, *17* (68), 165-174. DOI: https://doi.org/10.1016/j.rmu.2015.05.003.
(38) Bule, M., Khan, F., Niaz, K. *Antivirals: Past, Present and Future , bookTitle= Recent Advances in Animal Virology*; Springer Singapore, 2019. DOI: 10.1007/978-981-13-9073-9_22.

(39) Kausar, S.; Said Khan, F. A.-O.; Ishaq Mujeeb Ur Rehman, M.; Akram, M.; Riaz, M. A.-O.; Rasool, G.; Hamid Khan, A.; Saleem, I.; Shamim, S.; Malik, A. A review: Mechanism of action of antiviral drugs. (2058-7384 (Electronic)). From 2021 Jan-Dec.
(40) Wright, A. E.; Killday, K. B.; Chakrabarti, D.; Guzmán, E. A.; Harmody, D.; McCarthy, P. J.; Pitts, T.; Pomponi, S. A.; Reed, J. K.; Roberts, B. F.; et al. Dragmacidin G, a Bioactive Bis-Indole Alkaloid from a Deep-Water Sponge of the Genus *Spongosorites* . *Mar. Drugs* **2017**, *15* (16). DOI: 10.3390/md15010016.
(41) Cruz, P. G. a. M. L. J. F. a. D. A. H. a. P. M. a. C. C. On the Mechanism of Action of Dragmacidins I and J, Two New Representatives of a New Class of Protein Phosphatase 1 and 2A Inhibitors. *ACS Omega* **2018**, *3* (4), 3760-3767. DOI: 10.1021/acsomega.7b01786 , note = PMID: 30023878.
(42) Sandoz; A.G. Polymorph of rilpivirine hydrochloride and its use as antiviral.
(43) Gurjar; M.K.; Maikap, G. S.; JOSHI, S. G.; BADHE, S. A.; Samit, S. M. An improved rilpivirine process.
(44) Vasilakis, N.; Weaver, S. C. Flavivirus transmission focusing on Zika. (1879-6265 (Electronic)). From 2017 Feb.
(45) Pavan kommavarapu and Arthanareeswari Maruthapillai and Kamaraj Palanisamy and Manasvi, S. Preparation and characterization of rilpivirine solid dispersions with the application of enhanced solubility and dissolution rate. *Beni-Suef University Journal of Basic and Applied Sciences* **2015**, *4* (1), 71-79. DOI: https://doi.org/10.1016/j.bjbas.2015.02.010.
(46) Prakash Khadka and Jieun Ro and Hyeongmin Kim and Iksoo Kim and Jeong Tae Kim and Hyunil Kim and Jae Min Cho and Gyiae Yun and Jaehwi, L. Pharmaceutical particle technologies: An approach to improve drug solubility, dissolution and bioavailability. *Asian Journal of Pharmaceutical Sciences* **2014**, *9* (6), 304-316. DOI: https://doi.org/10.1016/j.ajps.2014.05.005.
(47) Prasad, V.; De Jesús, K.; Mailankody, S. The high price of anticancer drugs: origins, implications, barriers, solutions. (1759-4782 (Electronic)). From 2017 Jun.
(48) Alqahtani; M.S.; Kazi, M.; Alsenaidy, M. A.; Ahmad, M. Z. Advances in Oral Drug Delivery. *Front Pharmacol.* **2021**, *12*, 618411. DOI: 10.3389/fphar.2021.618411.
(49) Fernandes, J. a. G. C. R. Topological Polar Surface Area Defines Substrate Transport by Multidrug Resistance Associated Protein 1 (MRP1/ABCC1). *Journal of Medicinal Chemistry* **2009**, *52* (4), 1214-1218. DOI: 10.1021/jm801389m , note = PMID: 19193010.
(50) Ertl, P. a. R. B. a. S. P. Fast Calculation of Molecular Polar Surface Area as a Sum of Fragment-Based Contributions and Its Application to the Prediction of Drug Transport Properties. *Journal of Medicinal Chemistry* **2000**, *43* (20), 3714-3717. DOI: 10.1021/jm000942e, note = PMID: 11020286.
(51) Wei Xu, P. L., Tianmin Zhang. Polymeric Micelles, a Promising Drug Delivery System to Enhance Bioavailability of Poorly Water-Soluble Drugs. *Journal of Drug Delivery* **2013**, *2013*, 1-15. DOI: https://doi.org/10.1155/2013/340315.
(52) Prasanna, S.; Doerksen, R. J. Topological polar surface area: a useful descriptor in 2D-QSAR. (0929-8673 (Print)). From 2009.
(53) Catalano; A.; Iacopetta, D.; Ceramella, J.; Scumaci, D.; Giuzio, F.; Saturnino, C.; Aquaro, S.; Rosano, C.; Sinicropi, M. S. Multidrug Resistance (MDR): A Widespread Phenomenon in Pharmacological Therapies. *Molecules* **2022**, *27* (3), 616. DOI: 10.3390/molecules27030616.
(54) Tanwar, J.; Das, S. A.-O.; Fatima, Z.; Hameed, S. Multidrug resistance: an emerging crisis. (1687-708X (Print)). From 2014.

(55) Leonard; S.W.; Talebpour, S. Method of Compensation of Dose-Response Curve of an Assay for Sensitivity to Perturbing Variables.
(56) Copaescu; A.; Choshi, P.; Pedretti, S.; Mouhtouris, E.; Peter, J.; Trubiano, J. A. Dose Dependent Antimicrobial Cellular Cytotoxicity-Implications for ex vivo Diagnostics. *Front. Pharmacol.* **2021**, *12*, 640012. DOI: 10.3389/fphar.2021.640012.
(57) *Creating dose-response curves for cell-based and biochemical assays with the HP D300 Digital Dispenser*. https://cdn.technologynetworks.com/TN/Resources/PDF/Creating%20dose%20response%20curves%20for%20cell%20based%20and%20biochemical%20assays%20with%20the%20HP%20D300%20DigitalResponse.pdf (accessed February 10, 2023).
(58) Li; C.W.; Yang, J.; Yang, M. *Dose-dependent cell-based assays in V-shaped microfluidic channels*. 2006. (accessed 6 7).
(59) Larsson, P.; Engqvist, H.; Biermann, J.; Werner Rönnerman, E.; Forssell-Aronsson, E.; Kovács, A.; Karlsson, P.; Helou, K.; Parris, T. Z. Optimization of cell viability assays to improve replicability and reproducibility of cancer drug sensitivity screens. *Scientific Reports* **2020**, *10* (1), 5798. DOI: 10.1038/s41598-020-62848-5.
(60) Schwartz, H. R.; Richards, R.; Fontana, R. E.; Joyce, A. J.; Honeywell, M. E.; Lee, M. J. Drug GRADE: An Integrated Analysis of Population Growth and Cell Death Reveals Drug-Specific and Cancer Subtype-Specific Response Profiles. (2211-1247 (Electronic)). From 2020 Jun 23.
(61) Racaniello; V. *Renato Dulbecco, 1914-2012*. https://www.virology.ws/2012/02/23/renato-dulbecco-1914-2012/ (accessed December 23, 2022).
(62) Hunter; T. Renato Dulbecco: A Renaissance Scientist. *Cell* **2012**, *149* (1), 9-10. DOI: https://doi.org/10.1016/j.cell.2012.03.013.
(63) Dulbecco; R. Production of Plaques in Monolayer Tissue Cultures by Single Particles of an Animal Virus. *Proceedings of the National Academy of Sciences* **1952**, *38* (8), 747-752. DOI: DOI: 10.1002/cpmc.105.
(64) Mendoza, E. J. a. M. K. a. W. H. a. D. M. Two Detailed Plaque Assay Protocols for the Quantification of Infectious SARS-CoV-2. *Current Protocols in Microbiology* **2020**, *57* (1), cpmc105. DOI: https://doi.org/10.1002/cpmc.105.
(65) Racaniello; V. *Detecting viruses: the plaque assay*. https://www.virology.ws/2009/07/06/detecting-viruses-the-plaque-assay/ (accessed December 23, 2022).
(66) Crooke, S.; Whitlock, C. A General Synthesis of Bis-indolylpiperazine-2,5-diones. In *Molecules*, 2012; Vol. 17, pp 14841-14845.
(67) Christine, R. W. a. M. P. C. A total synthesis of dragmacidin B. *Tetrahedron Letters* **1994**, *35* (3), 371-374. DOI: https://doi.org/10.1016/0040-4039(94)85056-9.
(68) Ugiyadi; M.; Tan, M.; Giri Rachman, E.; Zuhairi, F.; Sumarsono, S. The expression of essential components for human influenza virus internalization in Vero and MDCK cells. *Cytotech.* **2013**, *66*, 515-523 DOI: https://doi.org/10.1007/s10616-013-9602-2.